Effects of interface-roughness scattering on nonlinear electron transport in a superlattice based on exact solution of generalized Boltzmann transport equation

Po-Hsin Shih,[1] Danhong Huang ◉,[2,*] Godfrey Gumbs ◉,[1,3] Thi-Nga Do ◉,[4] Christian P. Morath,[2] and T. Diana Maestas[2]

[1]*Department of Physics and Astronomy, Hunter College of the City University of New York, 695 Park Avenue, New York, New York 10065, USA*

[2]*Air Force Research Laboratory, Space Vehicles Directorate, Kirtland Air Force Base, New Mexico 87117, USA*

[3]*Donostia International Physics Center (DIPC), P de Manuel Lardizabal, 4, 20018 San Sebastian, Basque Country, Spain*

[4]*Department of Physics, National Cheng Kung University, Tainan 701, Taiwan*

In this paper, an effective scattering-potential approach is proposed for treating interface-roughness scattering of drifting electrons within a superlattice. By utilizing established effective scattering potentials, a quasi-one-dimensional generalized Boltzmann transport equation is developed after a self-consistent internal scattering force is included. This generalized Boltzmann transport equation is solved exactly afterwords beyond the relaxation-time approximation. Furthermore, the dependence of the resulting steady-state current on interface-roughness parameters is analyzed at various temperatures and dc electric-field strengths by utilizing the calculated nonequilibrium electron occupation function. Meanwhile, the microscopic mechanism behind non-ohmic transport behavior is revealed by analyzing numerically the computed nonequilibrium electron occupation function and its dependence on interface roughness parameters as well as the dc electric field strength.

I. INTRODUCTION

Vertical transport in superlattices (SLs) has gained considerable attention because of the unique band structures of type-II InAs/GaSb SLs which have appeared as third-generation infrared focal-plane arrays and photodiodes [1–10]. Meanwhile, the superior performance of such optoelectronic devices requires high carrier mobilities for efficient transport through drift and/or diffusion in the vertical direction [11]. However, vertical mobilities cannot be measured directly because their measurement involves nonstandard and indirect experimental techniques, e.g., the geometric magneto-resistance [12–15]. Consequently, the vertical mobility can only be extracted indirectly by fitting measured current-voltage data [16,17]. Historically, there have been a lot of published research works on in-plane transport within quantum wells [18], but there exists no comparable effort for SLs. Moreover, only limited measurements for SL transport have been performed [19], although the theory for diffusive carrier transport in SLs was developed a long time ago by Mori and Ando [20], as well as Dharssi and Butcher [21], and others [22,23]. Consequently, most theoretical and experimental works to date have still been limited to horizontal transport [24].

Notably, in a recent work by Szmulowicz *et al.* [25], a three-dimensional (3D) static theory was developed for numerically computing both vertical and horizontal mobilities of carriers at low temperatures within an InAs/GaSb SL, where a semi-classical Boltzmann transport theory is employed under a relaxation-time approximation and a very weak DC electric field. In our current quasi-one-dimensional

(1D) time-dependent theory, on the other hand, the scattering of electrons by interface roughness is calculated accurately beyond the relaxation-time approximation and the resulting nonlinear transport theory can be applied to a strong DC electric field and a large interface scattering of electrons. This leads to a field-dependent electron mobility beyond Ohm's law for a weak DC electric field only.

To the best of our knowledge, no exact solution for the Boltzmann transport equation has ever been analytically obtained so far with the full inclusion of microscopic scattering of electrons by impurities, phonons, or interface roughness. The electron dynamics of semiconductor SLs under a strong DC electric field $\mathcal{E}_0$ appears extremely rich due to the large number of parameters that can be controlled quite easily in experiments. As an example, evidence for Bloch oscillations in doped SLs, resulting in a negative differential conductance as predicted by Esaki and Tsu [26] was reported by Sibille *et al.* [14] for samples at both room and low temperatures. In such a situation, the tunable strong THz emitter enables real-time active spectral imaging in combination with a focal-plane photodetector array [27]. On the other hand, studies on long-time average current under AC monochromatic [28] and bichromatic [29] electric fields have also been reported recently. In those studies, the conditions for occurrence of dynamical localization [30–32] were shown either for a scattering-free system or within the relaxation-time approximation in the presence of elastic scattering. Meantime, conditions for generalized dynamical localization under AC electric fields were also displayed, when a tight-binding band structure beyond the nearest-neighbor approximation was employed [32,33].

In our current theory, instead of employing a relaxation-time approximation to deal with the scattering contributions in the Boltzmann transport equation [25], we adopt a

*danhong.huang@us.af.mil

first-principles quantum kinetic approach [34] for accurately capturing the full effects due to interface roughness on non-linear vertical transport of electrons in SLs. In addition, a scattering force is also included self-consistently in this formalism. To cut down on the computation time for these very complex and time consuming numerical computations, we construct effective 1D scattering potentials. Meanwhile, we also introduce the corresponding occupation function for nonequilibrium miniband electrons in their vertical SL transport subjected to both deflected and backward scattering of drifting electrons by in-plane interface roughness. Using this approach, we demonstrated the role of interface roughness in both DC and AC field-driven miniband transport [35]. Our quantum-kinetic theory enables evaluating accurately non-linear DC current and conductivity for vertical transport of miniband electrons in a SL by extracting its long-time steady-state values under a multistep function for setting up a DC electric field. In this work, we assume that the width $\mathcal{W}_0$ of a SL miniband is large and the applied DC electric field $\mathcal{E}_0$ is moderately high, so that the condition $e\mathcal{E}_0 d < \mathcal{W}_0$ can be satisfied to avoid Wannier-Stark localization of electrons in SLs [36,37].

The rest of this paper is organized as follows. In Sec. II, we put forward a first-principles quantum-kinetic model and introduce effective scattering potentials as well as 1D nonequilibrium occupation function for miniband electrons in SLs driven by DC/AC electric fields. Our study includes both deflected and backward scattering of electrons by in-plane interface roughness. Numerical results based on our quantum-kinetic theory for the transient current and nonequilibrium part of the drifting-electron occupation function in SLs are presented in Sec. III. Finally, a brief summary is given in Sec. IV along with some remarks.

II. EFFECT OF INTERFACE-ROUGHNESS SCATTERING

For studying an electrical current flowing through a SL structure in the presence of interface roughness, we propose the use of our previously developed generalized Boltzmann nonlinear-transport equation [34]. This gives rise to

$$\frac{d}{dt}f(\boldsymbol{k},t) = \frac{\partial f(\boldsymbol{k},t)}{\partial t}\bigg|_{\text{scat}} - \frac{\boldsymbol{F}_{\text{tot}}(k_z,t)}{\hbar} \cdot \frac{\partial f(\boldsymbol{k},t)}{\partial \boldsymbol{k}}, \quad (1)$$

where only one conduction miniband is considered in the electric-quantum limit for low electron volume density and thin barriers in SLs. In Eq. (1), $f(\boldsymbol{k},t)$ stands for a nonequilibrium occupation function for miniband electrons in a SL, $\boldsymbol{k} = \{\boldsymbol{k}_\parallel, k_z\}$ represents a three-dimensional wave vector of electrons, and $\boldsymbol{F}_{\text{tot}}(k_z,t)$ represents an applied transient force acting on both deflected and backward scattering of drifting electrons.

For Eq. (1), we would apply the Boltzmann-type scattering term to an ultrafast energy-relaxation process, giving rise to

$$\frac{\partial f(\boldsymbol{k},t)}{\partial t}\bigg|_{\text{scat}} = W_{\text{in}}(\boldsymbol{k},t\,|\,f)[1 - f(\boldsymbol{k},t)] - W_{\text{out}}(\boldsymbol{k},t\,|\,f)\,f(\boldsymbol{k},t)$$

$$\equiv W_{\text{in}}(\boldsymbol{k},t\,|\,f) - \frac{f(\boldsymbol{k},t)}{\tau_{\text{E}}(\boldsymbol{k})}, \quad (2)$$
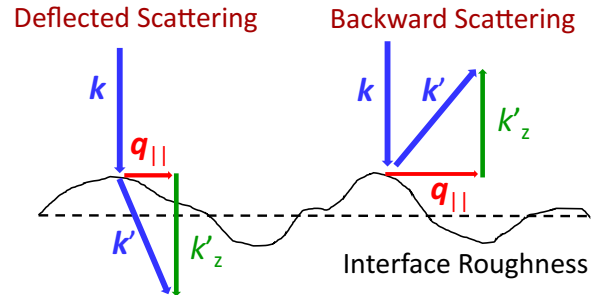

FIG. 1. Illustrations for deflected scattering (left with $k_z' > 0$), and backward scattering (right with $k_z' < 0$), by roughness (solid black curve) on an interface (black dashed line) within a superlattice structure, where $q_z = k_z' - k_z$, $\boldsymbol{q}_\parallel = \boldsymbol{k}_\parallel' - \boldsymbol{k}_\parallel$ are transition wave numbers and the total kinetic energy of electrons must be conserved for three-dimensional elastic-scattering events. Additionally, we must replace k_z' by $k_z' \pm 2\pi/d$ so as to maintain $|k_z'| \leqslant \pi/d$ within the first Brillouin zone for the Umklapp scattering with $|k_z'| > \pi/d$.

where $W_{\text{in}}(\boldsymbol{k},t\,|\,f)$ and $W_{\text{out}}(\boldsymbol{k},t\,|\,f)$ are, respectively. Here, the scattering-in and scattering-out rates for electrons with a wave vector $\boldsymbol{k}$ and are calculated as [34]

$$W_{\text{in}}(\boldsymbol{k},t\,|\,f) = \frac{2\pi}{\hbar}\sum_{\boldsymbol{k}'}|V_{\text{ds}}(\boldsymbol{k},\boldsymbol{k}')|^2\,f(\boldsymbol{k}',t)$$

$$\times\,\delta(\varepsilon_{\boldsymbol{k}} - \varepsilon_{\boldsymbol{k}'})\,\Theta[\tilde{\varepsilon}_{\boldsymbol{k}} - E_z(k_z')], \quad (3)$$

$$W_{\text{out}}(\boldsymbol{k},t\,|\,f) = \frac{2\pi}{\hbar}\sum_{\boldsymbol{k}'}|V_{\text{ds}}(\boldsymbol{k},\boldsymbol{k}')|^2[1 - f(\boldsymbol{k}',t)]$$

$$\times\,\delta(\varepsilon_{\boldsymbol{k}'} - \varepsilon_{\boldsymbol{k}})\,\Theta[\tilde{\varepsilon}_{\boldsymbol{k}} - E_z(k_z')], \quad (4)$$

and the inverse energy-relaxation time can be defined by

$$\frac{1}{\tau_{\text{E}}(\boldsymbol{k})} \equiv W_{\text{in}}(\boldsymbol{k},t\,|\,f) + W_{\text{out}}(\boldsymbol{k},t\,|\,f)$$

$$= \frac{2\pi}{\hbar}\sum_{\boldsymbol{k}'}|V_{\text{ds}}(\boldsymbol{k},\boldsymbol{k}')|^2\,\delta(\varepsilon_{\boldsymbol{k}} - \varepsilon_{\boldsymbol{k}'})\,\Theta[\tilde{\varepsilon}_{\boldsymbol{k}} - E_z(k_z')], \quad (5)$$

which is independent of occupation function $f(\boldsymbol{k},t)$. In Eqs. (3) and (4), $\varepsilon_{\boldsymbol{k}} \equiv \varepsilon_{\boldsymbol{k}_\parallel, k_z} = \hbar\Omega_0/2 + \hbar^2 k_\parallel^2/2m^* + \mathcal{W}_0\sin^2(k_z d/2)$ represents the kinetic energy for the lowest-miniband electrons in a type-I SL with a spatial period d, an isotropic in-plane effective mass m^*, a tight-binding miniband width $\mathcal{W}_0$, and a harmonic frequency Ω_0 due to quantum-well confinement, and $\tilde{\varepsilon}_{\boldsymbol{k}} = \varepsilon_{\boldsymbol{k}} - \hbar\Omega_0/2$. In addition, $E_z(k_z) \equiv \mathcal{W}_0\sin^2(k_z d/2)$, and $\Theta(x)$ represents an unity-step function to ensure a real-value wave vector $k_\parallel'$ [23,25]. Furthermore, both electron-electron and electron-phonon scattering have been neglected for low doping densities and temperatures. The summations over $\boldsymbol{k}'$ in Eqs. (3) and (4) should exclude the term with $\boldsymbol{k}' = \boldsymbol{k}$. Moreover, $|V_{\text{ds}}(\boldsymbol{k},\boldsymbol{k}')|^2$ in Eq. (5) is the scattering potential for dominant deflected ($k_z' > 0$) and second backward ($k_z' < 0$) elastic scattering [38] of miniband electrons by interface roughness within a SL structure, as illustrated in Fig. 1, and is calculated explicitly as [25]

$$|V_{\text{ds}}(\boldsymbol{k},\boldsymbol{k}')|^2 = \frac{2\pi V_0^2 \Delta_0^2 \Lambda_0^2}{\mathcal{A}}\,\text{e}^{-q_\parallel^2 \Lambda_0^2/4}\big|\phi_{k_z'}^{\text{SL}}(a)\big|^2\big|\phi_{k_z}^{\text{SL}}(a)\big|^2. \quad (6)$$

In Eq. (6), roughness at both interfaces of a quantum well is included, $q = k' - k$ is a transition wave vector for dominant deflected/second backward electron scattering illustrated in Fig. 1, V_0 is the depth of a symmetrical quantum well for conduction electrons located at the right edge $z = a$ (or equivalently, at the left edge $z = -a$), Δ_0 is the average amplitude for interface roughness, Λ_0 is the in-plane correlation length for interface roughness, $\mathcal{A}$ is the cross-sectional area of SLs, and $\phi_{k_z}^{\mathrm{SL}}(z)$ stands for the z component of a SL wave function $\Psi_{\mathbf{k}}^{\mathrm{SL}}(\mathbf{r}) \equiv \Psi_{\mathbf{k}_\parallel, k_z}^{\mathrm{SL}}(\mathbf{r}_\parallel, z) = [\exp(i\mathbf{k}_\parallel \cdot \mathbf{r}_\parallel)/\sqrt{\mathcal{A}}] \, \phi_{k_z}^{\mathrm{SL}}(z)$. Different from the in-plane transport, the interface-roughness scattering for vertical transport is a three-dimensional process intrinsically. Within the 1D tight-binding model, $\phi_{k_z}^{\mathrm{SL}}(z)$ is written as [39]

$$\phi_{k_z}^{\mathrm{SL}}(z) = \frac{1}{\sqrt{N_0 + 1}} \sum_{j=-N_0/2}^{N_0/2} e^{ik_z jd} \, \chi_0^{\mathrm{QW}}(z - jd) = \left[\phi_{-k_z}^{\mathrm{SL}}(z)\right]^*, \tag{7}$$

where $N_0 + 1$ represents the total number of unit cells in the SL, and the individual quantum-well ground-state wave function takes the form $|\chi_0^{\mathrm{QW}}(z)|^2 = (1/\sigma\sqrt{2\pi}) \exp(-z^2/2\sigma^2)$ with $\sigma \lesssim a < d/2$ for weak tunneling of electrons. In Eqs. (3) to (5), the so-called Umklapp-scattering process [40] with $|k_z' - k_z| > \pi/d$ could occur. To include this Umklapp-scattering effect, we must replace k_z' by $k_z' \pm 2\pi/d$ properly to ensure that the new final scattering-transition wave number $k_z' \pm 2\pi/d$ always stays within the first Brillouin zone $[-\pi/d, \pi/d]$.

In Eq. (6), we assumed that the dominant contribution for scattering of electrons in SLs comes from the interface roughness, while the electron-electron [41] and electron-phonon [42] scattering are expected small for low doping density and temperatures, respectively. To investigate the vertical transport of miniband electrons in SLs, we consider the total transient force $\mathbf{F}_{\mathrm{tot}}(k_z, t) = \mathcal{F}_{\mathrm{tot}}(k_z, t) \hat{\mathbf{e}}_z$ pointing towards the z (or SL) direction. Here, to greatly cut down numerical computations, we formally introduce an effective 1D occupation function $n(k_z, t)$ for nonequilibrium miniband electrons only, defined by

$$n(k_z, t) \equiv \frac{2}{n_{\mathrm{qw}}\mathcal{A}} \sum_{\mathbf{k}_\parallel} f(\mathbf{k}, t)$$

$$\approx \frac{1}{2\pi^2 \rho_0 d} \int d^2 \mathbf{k}_\parallel \, f(\{\mathbf{k}_\parallel, k_z\}, t), \tag{8}$$

where the two-fold spin degeneracy of electrons is included, the areal density $n_{\mathrm{qw}} \approx \rho_0 d$ for electrons in individual quantum well is given by Eq. (26) below since the total number of electrons in a SL system remains to be a constant in transport and ρ_0 is the volume density for electrons from remote doping of SLs.

In a recent work by Szmulowicz *et al.* [25] a 3D static-transport theory was developed for semi-analytically computing both vertical and horizontal mobilities of carriers at low temperatures within an InAs/GaSb SL, where a semi-classical Boltzmann transport theory is employed along with a relaxation-time approximation and an assumption of a very weak DC electric field. In our current quasi-1D

time-dependent theory, on the other hand, the scattering of electrons by interface roughness is calculated accurately beyond the relaxation-time approximation and the resulting nonlinear transport theory can be applied to strong DC electric field and interface scattering of electrons, leading to a field-dependent electron mobility beyond Ohm's law under a weak DC electric field only.

Generally speaking, the current physics model with an effective 1D scattering potential holds true for a system with an anisotropic band structure, such as a superlattice, as well as a driving motion and a strong scattering of electrons in parallel and perpendicular to the SL direction, respectively. Specifically, if we assume that the condition $|\Delta k_z| \equiv e\mathcal{E}_0 d/\hbar|v_d| \gg 1/\Lambda_0 > |\mathbf{q}_\parallel|$ is satisfied by electrons in this SL system, then the correlation between the vertical and parallel motions within a SL is expected very weak, where $\mathcal{E}_0$, d, v_d, and Λ_0 represent DC electric-field strength, superlattice period, drift velocity of electrons, and correlation length of interface roughness, respectively. As a result, the full occupation function can be approximately factorized into individual in-plane and vertical components. Meanwhile, the small transferred in-plane momentum from initially fast-driving electrons along the SL direction will be quickly balanced by strong interface-roughness scattering of electrons within a quantum well and maintain a thermal-equilibrium state. In this way, an effective 1D scattering potential can be validated.

Under this assumption, Eq. (1) can now be projected onto this 1D k_z-space ($|k_z| \leqslant \pi/d$) as

$$\frac{d}{dt}\Delta n(k_z, t) = \left.\frac{\partial n(k_z, t)}{\partial t}\right|_{\mathrm{scat}} - \frac{\mathcal{F}_{\mathrm{tot}}(k_z, t)}{\hbar}\left[\frac{\partial n_0(k_z)}{\partial k_z} + \frac{\partial \Delta n(k_z, t)}{\partial k_z}\right], \tag{9}$$

where $\Delta n(k_z, t) \equiv n(k_z, t) - n_0(k_z)$ describes the nonequilibrium part of electron occupation function due to applied DC electric field, while $n_0(k_z)$ is the initial thermal-equilibrium occupation of electrons given by Eq. (25) below. It is important to notice that the electric current flowing within a SL only relies on $\Delta n(k_z, t)$ but not on $n_0(k_z)$. Mathematically, Eq. (9) can be utilized to evaluate the next-time nonequilibrium distribution $\Delta n(k_z, t + \Delta t)$ for $|k_z| < \pi/d$ (besides two points at $k_z = \pm\pi/d$) based on a so-called three-point central-difference approach [35] for the drifting term $\partial \Delta n(k_z, t)/\partial k_z$ as well as known values of $\Delta n(k_z, t)$ at previous time t. However, the value of $n(k_z = \pm\pi/d, t + \Delta t)$ should still be determined by the following restraint equation for the conservation of total number of electrons within a SL [35], that is,

$$\frac{d}{2\pi}\int_{-\pi/d}^{\pi/d} dk_z \, \Delta n(k_z, t + \Delta t) \equiv 0. \tag{10}$$

Therefore, we expect that $\Delta n(k_z = \pm\pi/d, t + \Delta t)$ at two Brillouin-zone boundary points can be expressed by $\Delta n(k_z, t + \Delta t)$ within the range of $|k_z| < \pi/d$, which is explicitly given by

$$g_1(t + \Delta t) = g_N(t + \Delta t) = -\frac{1}{2}\sum_{j=2}^{N-1} g_j(t + \Delta t), \tag{11}$$

from which we always get

$$\sum_{j=1}^{N} g_j(t + \Delta t) \equiv 0, \tag{12}$$

where $g_j(t + \Delta t) \equiv \Delta n(k_j, t + \Delta t)$ for $1 \leqslant j \leqslant N$, $k_j = -\pi/d + (j - 1)\Delta k$, $\Delta k = 2\pi/(N - 1)d$, and $N > 3$ is an integer representing a total number of equal-distance discrete

points within the first Brillouin zone of a SL. Here, we want to emphasize that our calculated $\Delta n(k_z, t)$ from Eq. (9) will generally satisfy $\Delta n(k_z, t) \neq \Delta n(-k_z, t)$ for $|k_z| < \pi/d$ under a finite DC electric field although $\Delta n(k_z = \pi/d, t) = \Delta n(k_z = -\pi/d, t)$ is always maintained.

By applying the detailed-balance condition, we introduced in Eq. (9) a reduced Boltzmann-type scattering term on its right-hand side, given by

$$\frac{\partial n(k_z, t)}{\partial t}\bigg|_{\text{scat}} \approx \frac{2}{n_{\text{qw}}\mathcal{A}} \sum_{\mathbf{k}_\parallel} \frac{\partial f(\{\mathbf{k}_\parallel, k_z\}, t)}{\partial t}\bigg|_{\text{scat}}^{\text{(in)}} [1 - f_0(E_{xy}(k_\parallel) - \mu_0)] - \frac{2}{n_{\text{qw}}\mathcal{A}} \sum_{\mathbf{k}_\parallel} \frac{\partial f(\{\mathbf{k}_\parallel, k_z\}, t)}{\partial t}\bigg|_{\text{scat}}^{\text{(out)}} f_0(E_{xy}(k_\parallel) - \mu_0)$$

$$\equiv \mathcal{W}_{\text{in}}(k_z, t \mid n_0 + \Delta n)[1 - n_0(k_z) - \Delta n(k_z, t)] - \mathcal{W}_{\text{out}}(k_z, t \mid n_0 + \Delta n)[n_0(k_z) + \Delta n(k_z, t)]$$

$$- \delta_{t,0} \left[\mathcal{W}_{\text{in}}^{(0)}(k_z \mid n_0)[1 - n_0(k_z)] - \mathcal{W}_{\text{out}}^{(0)}(k_z \mid n_0) n_0(k_z) \right], \tag{13}$$

where the detailed-balance condition has been employed for initial state $n(k_z, t = 0) \equiv n_0(k_z)$, and the reduced 1D scattering-in and scattering-out rates are written as

$$\mathcal{W}_{\text{in}}(k_z, t \mid n_0 + \Delta n) \approx \frac{2}{n_{\text{qw}}\mathcal{A}} \sum_{\mathbf{k}_\parallel} W_{\text{in}}(\mathbf{k}, t \mid f)[1 - f_0(E_{xy}(k_\parallel) - \mu_0)] \equiv \frac{2\pi}{\hbar} \sum_{k_z'} U_{\text{sc}}^{\text{(in)}}(k_z, k_z')[n_0(k_z') + \Delta n(k_z', t)]$$

$$= \frac{U_{\text{m}} d}{\hbar} \int_{-\pi/d}^{\pi/d} dk_z' \, \overline{U}_{\text{sc}}^{\text{(in)}}(k_z, k_z')[n_0(k_z') + \Delta n(k_z', t)], \tag{14}$$

$$\mathcal{W}_{\text{out}}(k_z, t \mid n_0 + \Delta n) \approx \frac{2}{n_{\text{qw}}\mathcal{A}} \sum_{\mathbf{k}_\parallel} W_{\text{out}}(\mathbf{k}, t \mid f) f_0(E_{xy}(k_\parallel) - \mu_0) \equiv \frac{2\pi}{\hbar} \sum_{k_z'} U_{\text{sc}}^{\text{(out)}}(k_z, k_z')[1 - n_0(k_z') - \Delta n(k_z', t)]$$

$$= \frac{U_{\text{m}} d}{\hbar} \int_{-\pi/d}^{\pi/d} dk_z' \, \overline{U}_{\text{sc}}^{\text{(out)}}(k_z, k_z')[1 - n_0(k_z') - \Delta n(k_z', t)], \tag{15}$$

and $\mathcal{W}_{\text{in}}^{(0)}(k_z \mid n_0)$ and $\mathcal{W}_{\text{out}}^{(0)}(k_z \mid n_0)$ can be obtained from Eqs. (14) and (15), correspondingly, simply by setting $\Delta n(k_z', t) = 0$. In Eq. (13), we employed an ansatz by inserting a thermal-equilibrium distribution $f_0[E_{xy}(k_\parallel) - \mu_0]$ for the inclusion of in-plane scattering contributions through an average over all in-plane scattering states. In Eqs. (13) to (15), we used an implicit energy drain for the transversal degrees of freedom of electrons so as to keep them in a thermal-equilibrium state. Here, $f_0[E_{xy}(k_\parallel) - \mu_0] = \{1 + \exp[((E_{xy}(k_\parallel) - \mu_0(T))/k_B T]\}^{-1}$ in Eqs. (14) and (15), which also appears in Eqs. (16) and (17) below, approaches $\Theta[E_F - E_{xy}(k_\parallel)]$ with Fermi energy E_F at low temperatures $k_B T \ll E_F$, where $E_{xy}(k_\parallel) = \hbar\Omega_0/2 + \hbar^2 k_\parallel^2/2m^*$. In Eqs. (14) and (15), we denote $\overline{U}_{\text{sc}}(k_z, k_z') \equiv U_{\text{sc}}(k_z, k_z')/U_{\text{m}}$ with a scaled value U_{m} for the maximum of function $|U_{\text{sc}}(k_z, k_z')|$, and meanwhile we require mathematically that the time change Δt, initially introduced in Eq. (11), satisfies $\Delta t \ll U_{\text{m}}/\hbar$. Importantly, Eq. (13) becomes nonlinear with $\Delta n(k_z, t)$ since $\mathcal{W}_{\text{in}}$ and $\mathcal{W}_{\text{out}}$ depend on $n(k_z, t)$, and Eq. (9) can be approximated by a differential matrix equation if all the higher-order terms $\propto [\Delta n(k_z, t)]^2$ are neglected [35].

Moreover, by applying conservation of the total kinetic energy of electrons for elastic scattering, the inelastic-scattering potential $U_{\text{sc}}(k_z, k_z')$, in Eqs. (14) and (15), takes the explicit forms

$$U_{\text{sc}}^{\text{(in)}}(k_z, k_z') = \frac{2}{n_{\text{qw}}\mathcal{A}} \sum_{\mathbf{k}_\parallel, \mathbf{k}_\parallel'} |V_{\text{ds}}(\mathbf{k}, \mathbf{k}')|^2 \delta(\varepsilon_{\mathbf{k}} - \varepsilon_{\mathbf{k}'}) \Theta[\tilde{\varepsilon}_{\mathbf{k}_\parallel, k_z} - E_z(k_z')][1 - f_0(E_{xy}(k_\parallel) - \mu_0)] f_0(E_{xy}(k_\parallel') - \mu_0)$$

$$\approx \frac{4\pi V_0^2 \Delta_0^2 \Lambda_0^2}{n_{\text{qw}}} \left|\phi_{k_z'}^{\text{SL}}(a)\right|^2 \left|\phi_{k_z}^{\text{SL}}(a)\right|^2 \frac{1}{\mathcal{A}^2} \sum_{\mathbf{k}_\parallel} [1 - f_0(E_{xy}(k_\parallel) - \mu_0)] \Theta[\tilde{\varepsilon}_{\mathbf{k}_\parallel, k_z} - E_z(k_z')]$$

$$\times \sum_{\mathbf{k}_\parallel'} \exp\left(-\frac{1}{4}|\mathbf{k}_\parallel - \mathbf{k}_\parallel'|^2 \Lambda_0^2\right) \delta(\varepsilon_{\mathbf{k}_\parallel, k_z} - \varepsilon_{\mathbf{k}_\parallel', k_z'}) f_0[E_{xy}(k_\parallel') - \mu_0]$$

$$\approx \frac{V_0^2 \Delta_0^2 \Lambda_0^2}{2\pi^2 n_{\text{qw}}} \left|\chi_0^{\text{QW}}(a)\right|^4 \int_0^\infty dk_\parallel \, k_\parallel \{1 - f_0[E_{xy}(k_\parallel) - \mu_0]\} \Theta[\tilde{\varepsilon}_{\mathbf{k}_\parallel, k_z} - E_z(k_z')]$$

$$\times \int_0^\infty dk_\parallel' \, k_\parallel' \mathcal{L}_0(\varepsilon_{\mathbf{k}_\parallel, k_z} - \varepsilon_{\mathbf{k}_\parallel', k_z'}, \hbar\Gamma_0) \int_0^{2\pi} d\theta_0 \exp\left[-\frac{\mathcal{P}_0(k_\parallel, k_\parallel', \theta_0)\Lambda_0^2}{4}\right] f_0[E_{xy}(k_\parallel') - \mu_0], \tag{16}$$

$$U_{\text{sc}}^{(\text{out})}(k_z, k_z') = \frac{2}{n_{\text{qw}}\mathcal{A}} \sum_{\mathbf{k}_\parallel, \mathbf{k}_\parallel'} |V_{\text{ds}}(\boldsymbol{k}, \boldsymbol{k}')|^2 \, \delta(\varepsilon_{\mathbf{k}} - \varepsilon_{\mathbf{k}'}) \, \Theta[\tilde{\varepsilon}_{\mathbf{k}_\parallel, k_z} - E_z(k_z')] \, f_0[E_{xy}(k_\parallel) - \mu_0] \, [1 - f_0(E_{xy}(k_\parallel') - \mu_0)]$$

$$\approx \frac{4\pi V_0^2 \Delta_0^2 \Lambda_0^2}{n_{\text{qw}}} |\phi_{k_z'}^{\text{SL}}(a)|^2 \, |\phi_{k_z}^{\text{SL}}(a)|^2 \frac{1}{\mathcal{A}^2} \sum_{\mathbf{k}_\parallel} f_0[E_{xy}(k_\parallel) - \mu_0] \, \Theta[\tilde{\varepsilon}_{\mathbf{k}_\parallel, k_z} - E_z(k_z')]$$

$$\times \sum_{\mathbf{k}_\parallel'} \exp\left(-\frac{1}{4} |\boldsymbol{k}_\parallel - \boldsymbol{k}_\parallel'|^2 \Lambda_0^2\right) \delta(\varepsilon_{\mathbf{k}_\parallel, k_z} - \varepsilon_{\mathbf{k}_\parallel', k_z'}) \{1 - f_0[E_{xy}(k_\parallel') - \mu_0]\}$$

$$\approx \frac{V_0^2 \Delta_0^2 \Lambda_0^2}{2\pi^2 n_{\text{qw}}} |\chi_0^{\text{QW}}(a)|^4 \int_0^\infty dk_\parallel \, k_\parallel \, f_0[E_{xy}(k_\parallel) - \mu_0] \, \Theta[\tilde{\varepsilon}_{\mathbf{k}_\parallel, k_z} - E_z(k_z')]$$

$$\times \int_0^\infty dk_\parallel' \, k_\parallel' \mathcal{L}_0(\varepsilon_{\mathbf{k}_\parallel, k_z} - \varepsilon_{\mathbf{k}_\parallel', k_z'}, \, \hbar\Gamma_0) \int_0^{2\pi} d\theta_0 \, \exp\left[-\frac{\mathcal{P}_0(k_\parallel, k_\parallel', \theta_0)\Lambda_0^2}{4}\right] \{1 - f_0[E_{xy}(k_\parallel') - \mu_0]\}. \tag{17}$$

In Eqs. (16) and (17), $\mathcal{P}_0(k_\parallel, k_\parallel', \theta_0) = k_\parallel^2 + k_\parallel'^2 - 2k_\parallel k_\parallel' \cos\theta_0 \geqslant 0$ while θ_0 is the angle between $\boldsymbol{k}_\parallel$ and $\boldsymbol{k}_\parallel'$, $U_{\text{sc}}^{(\text{out})}(k_z, k_z') = U_{\text{sc}}^{(\text{out})}(k_z, -k_z') = U_{\text{sc}}^{(\text{out})}(-k_z, k_z')$ for randomized scattering, and $|\chi_0^{\text{QW}}(a)| = |\chi_0^{\text{QW}}(-a)|$ for a symmetrical quantum well. Moreover, in Eqs. (16) and (17), $U_{\text{sc}}(k_z, k_z') \geqslant 0$, $\mathcal{L}_0(a, b) = b/[\pi(a^2 + b^2)]$ is the Lorentz-shape function, Γ_0 ($\ll \mathcal{W}_0/\hbar$) is the inverse-lifetime broadening of conduction electrons, $\tilde{\varepsilon}_{\mathbf{k}_\parallel, k_z} \equiv \varepsilon_{\mathbf{k}_\parallel, k_z} - \hbar\Omega_0/2 = E_{xy}(k_\parallel) - \hbar\Omega_0/2 + \mathcal{W}_0 \sin^2(k_z d/2) \equiv \tilde{E}_{xy}(k_\parallel) + E_z(k_z)$ represents the total-energy dispersion for miniband electrons with nearest-neighbor coupling in an 1D tight-binding model, and the variable in Lorentz-shape function is calculated explicitly as $\tilde{\varepsilon}_{\mathbf{k}_\parallel, k_z} - \tilde{\varepsilon}_{\mathbf{k}_\parallel', k_z'} = [E_z(k_z) - E_z(k_z')] + [\tilde{E}_{xy}(k_\parallel) - \tilde{E}_{xy}(k_\parallel')]$. Here, only the total kinetic energy of scattering electrons in Eqs. (16) and (17) is required to be conserved but not the individual ones in either the longitudinal or transverse direction. Furthermore, we will employ the relations $k_\parallel dk_\parallel = (m^*/\hbar^2) \, d\tilde{E}_{xy}(k_\parallel)$ and $dk_z' = (2/\mathcal{W}_0 d) \, dE_z(k_z')/\sqrt{1 - \{1 - (2/\mathcal{W}_0)[E_z(k_z') + \hbar\Gamma_0]\}^2}$ for computations in Eqs. (16) and (17), where $\tilde{E}_{xy}(k_\parallel) = \hbar^2 k_\parallel^2/2m^*$ and $E_z(k_z') = \mathcal{W}_0 \sin^2(k_z' d/2)$. From Eqs. (16) and (17), we realize that such a 3D scattering process, as illustrated in Fig. 1, can be effectively viewed as an 1D one after an average with respect to the in-plane scattering contributions of electrons has been performed.

For Eqs. (16) and (17), we would like to point out that the obtained reduced-form scattering potentials $U_{\text{sc}}^{(\text{in})}(k_z, k_z')$

and $U_{\text{sc}}^{(\text{out})}(k_z, k_z')$, which are associated with initial-/final-state electron wave numbers k_z and k_z' in a quasi-1D SL system, actually represent an inelastic-scattering process for SL electrons with respect to wave numbers k_z and k_z' although its original form with an anisotropic energy dispersion is indeed an elastic-scattering process for electrons in a 3D bulk system. Particularly, if a one-dimensional elastic-scattering process is assumed for electrons in a SL, we are simply left with $k_z' = -k_z$.

For the total transient force $\mathcal{F}_{\text{tot}}(k_z, t)$, lying along the SL ($z$) direction, on the left-hand side of Eq. (9), we include an inhomogeneous k_z-dependent scattering (or resistive) force, i.e.,

$$\mathcal{F}_{\text{tot}}(k_z, t) = -\frac{e\mathcal{E}_0}{M} \sum_{j=1}^M \left[\frac{1}{2} + \frac{1}{\pi} \tan^{-1}\left(\frac{t - j\Delta t}{\delta_0}\right)\right]$$
$$+ f_{\text{res}}(k_z, t), \tag{18}$$

where, for the first term on its right-hand side, M is the number of turning-on steps, Δt is the step-delayed time, $\mathcal{E}_0$ ($e\mathcal{E}_0 d < \mathcal{W}_0$) is the magnitude of a DC electric field, $t_j = j\Delta t$ is the jth turning-on time, Δt is the waiting (or stage) time, and δ_0 ($\ll \Delta t$) represents the broadening for a turning-on time at $t = t_j$. On the other hand, the k_z-dependent dynamical scattering force $f_{\text{res}}(k_z, t)$ in Eq. (18) results from momentum dissipation of drift electrons in the presence of interface-roughness scattering, yielding [34,43,44]

$$f_{\text{res}}(k_z, t) = \hbar \sum_{k_z'} (k_z' - k_z) \, \Xi_s^{(+)}(k_z, k_z'; t \mid n) \, \Theta(k_z' - k_z) + \hbar \sum_{k_z'} (k_z - k_z') \, \Xi_s^{(-)}(k_z, k_z'; t \mid n) \, \Theta(k_z - k_z')$$

$$= \frac{\hbar d}{2\pi} \left[\int_{-\pi/d}^{\pi/d} dk_z' \, (k_z' - k_z) \, \Xi_s^{(+)}(k_z', k_z; t \mid n) \, \Theta(k_z' - k_z) + \int_{-\pi/d}^{\pi/d} dk_z' \, (k_z - k_z') \, \Xi_s^{(-)}(k_z, k_z'; t \mid n) \, \Theta(k_z - k_z')\right], \tag{19}$$

where the scattering-in (+) and scattering-out (−) rates for momentum dissipation of drifting electrons are given, respectively, by

$$\Xi_s^{(+)}(k_z, k'_z; t \mid n) = \frac{2\pi}{\hbar} U_{\text{sc}}^{(\text{in})}(k_z, k'_z) [n_0(k'_z) + \Delta n(k'_z, t)] [1 - n_0(k_z) - \Delta n(k_z, t)] - \frac{2\pi}{\hbar} U_{\text{sc}}^{(\text{in})}(k_z, k'_z) n_0(k'_z) [1 - n_0(k_z)]$$

$$\approx \frac{2\pi}{\hbar} U_{\text{sc}}^{(\text{in})}(k_z, k_z + q_z) \{\Delta n(k_z + q_z, t) [1 - n_0(k_z)] - n_0(k_z + q_z) \Delta n(k_z, t)\} + \mathcal{O}(\Delta n)^2, \tag{20}$$

$$\Xi_s^{(-)}(k_z, k'_z; t \mid n) = \frac{2\pi}{\hbar} U_{\text{sc}}^{(\text{out})}(k_z, k'_z) [n_0(k_z) + \Delta n(k_z, t)] [1 - n_0(k'_z) - \Delta n(k'_z, t)] - \frac{2\pi}{\hbar} U_{\text{sc}}^{(\text{out})}(k_z, k'_z) n_0(k_z) [1 - n_0(k'_z)]$$

$$\approx \frac{2\pi}{\hbar} U_{\text{sc}}^{(\text{out})}(k_z, k_z - q_z) \{\Delta n(k_z, t) [1 - n_0(k_z - q_z)] - n_0(k_z) \Delta n(k_z - q_z, t)\} + \mathcal{O}(\Delta n)^2. \tag{21}$$

Here, we set $k'_z = k_z + q_z$ and $k'_z = k_z - q_z$, respectively, with $q_z \geqslant 0$ in Eqs. (20) and (21) at their last steps for a DC electric field $\mathcal{E}_0$ pointing in the z direction.

Physically, the dynamical force $f_{\text{res}}(k_z, t)$ introduced in Eq. (19) is zero at initial time $t = 0$ for a thermal-equilibrium distribution of electrons and plays a role for reducing a nonequilibrium distribution function $\Delta n(k_z, t)$ shifted towards negative k_z direction by accelerated electrons under a DC electric field $\mathcal{E}_0$. Furthermore, as seen in Eqs. (20) and (21), this scattering force $f_{\text{res}}(k_z, t)$, which excludes a nonlinear term $\sim \mathcal{O}(\Delta n)^2$ for electron transport within the first Brillouin zone in SLs, should be determined self-consistently with respect to $\Delta n(k_z, t)$ and will give rise to slight joule heating (different from thermal heating) to drifting electrons.

For simplicity, if we assume $|q_z/k_z| \ll 1$ for dominant small-angle vertical scattering events, Eqs. (20) and (21) simply reduce to

$$\Xi_s^{(+)}(k_z, k_z + q_z; t \mid n) + \Xi_s^{(-)}(k_z, k_z - q_z; t \mid n) \approx \frac{2\pi}{\hbar} U_{\text{av}}(k_z) \left[2\Delta n(k_z, t) [1 - 2n_0(k_z)] + q_z \frac{\partial \Delta n(k_z, t)}{\partial k_z} \right], \tag{22}$$

where the average scattering potential amplitude $U_{\text{av}}(k_z)$ is defined by

$$U_{\text{av}}(k_z) = \frac{d}{\pi} \int_0^{\pi/d} dq_z \left[U_{\text{sc}}^{(\text{in})}(k_z, k_z + q_z) + U_{\text{sc}}^{(\text{out})}(k_z, k_z - q_z) \right] > 0. \tag{23}$$

In Eq. (23), $k_z \pm q_z$ are supposed to be limited within the first Brillouin zone $[-\pi/d, \pi/d]$, which can be ensured by adjusting them into $k_z + q_z \pm 2\pi/d$ and $k_z - q_z \pm 2\pi/d$, respectively, if $|k_z \pm q_z| > \pi/d$, i.e., the so-called Umklapp scattering effect. Therefore, by combining Eqs. (19) with (22), we finally arrive at an expression for the k_z-dependent dynamical scattering force, i.e.,

$$f_{\text{res}}(k_z, t) \approx U_{\text{av}}(k_z) d \int_0^{\pi/d} dq_z\, q_z \left[2\Delta n(k_z, t) [1 - 2n_0(k_z)] + q_z \frac{\partial \Delta n(k_z, t)}{\partial k_z} \right]$$

$$= \frac{\pi^2 U_{\text{av}}(k_z)}{d} \left[\Delta n(k_z, t) [1 - 2n_0(k_z)] + \frac{1}{3} \left(\frac{\pi}{d} \right) \frac{\partial \Delta n(k_z, t)}{\partial k_z} \right], \tag{24}$$

which appears with an opposite sign in comparison with the first term in Eq. (18) for an applied DC electric force. Mathematically speaking, since $\partial \Delta n(k_z, t)/\partial k_z > 0$ and $\Delta n(k_z, t) > 0$ for $k_z < 0$, we know from Eq. (24) that $f_{\text{res}}(k_z, t) > 0$. In this case, the positive $f_{\text{res}}(k_z, t)$ can reduce the effect of a DC electric field $\mathcal{E}_0$ along the positive k_z direction. On the other hand, we find $f_{\text{res}}(k_z, t) < 0$ for $k_z > 0$ because of $\partial \Delta n(k_z, t)/\partial k_z < 0$ and $\Delta n(k_z, t) \approx 0$. From Eq. (9), we further realize that the scattering-force correction term $f_{\text{res}}(k_z, t)$ contributes to the Boltzmann transport equation by including two new nonlinear driving terms proportional to $\sim \{\Delta n(k_z, t),\, \partial \Delta n(k_z, t)/\partial k_z\} \times [\partial n_0(k_z)/\partial k_z + \partial \Delta n(k_z, t)/\partial k_z] \propto \mathcal{O}\{\Delta n(k_z, t)\partial \Delta n(k_z, t)/\partial k_z,\, [\partial \Delta n(k_z, t)/\partial k_z]^2\}$, which is expected to reduce the effect of an applied $\mathcal{E}_0$ pointing towards the positive k_z direction.

Since DC electric field is applied only after $t = 0$, the initial condition for occupation function $n(k_z, t)$ at $t = 0$ can be simply set as a thermal-equilibrium Fermi function at temperature T_0, that is,

$$n_0(k_z) \equiv n(k_z, t = 0) = \frac{2}{n_{\text{qw}} \mathcal{A}} \sum_{\mathbf{k}_\parallel} \left\{ 1 + \exp \left[\frac{\varepsilon_{\mathbf{k}_\parallel, k_z} - \mu_0(T_0)}{k_B T_0} \right] \right\}^{-1}$$

$$= \frac{1}{\pi n_{\text{qw}}} \int_0^\infty dk_\parallel\, k_\parallel \left\{ 1 + \exp \left[\frac{\varepsilon_{\mathbf{k}_\parallel, k_z} - \mu_0(T_0)}{k_B T_0} \right] \right\}^{-1}, \tag{25}$$

or $\Delta n(k_z, t = 0) = 0$, where $\mu_0(T_0)$ is the chemical potential, which, for a given volume doping density ρ_0, is determined by the root of the following constraint equation [45] for any fixed value of T_0, i.e.,

$$\rho_0 = \frac{1}{2\pi^2} \int_{-\pi/d}^{\pi/d} dk_z \int_0^\infty dk_\parallel\, k_\parallel \left\{ 1 + \exp \left[\frac{\varepsilon_{\mathbf{k}_\parallel, k_z} - \mu_0(T_0)}{k_B T_0} \right] \right\}^{-1}. \tag{26}$$
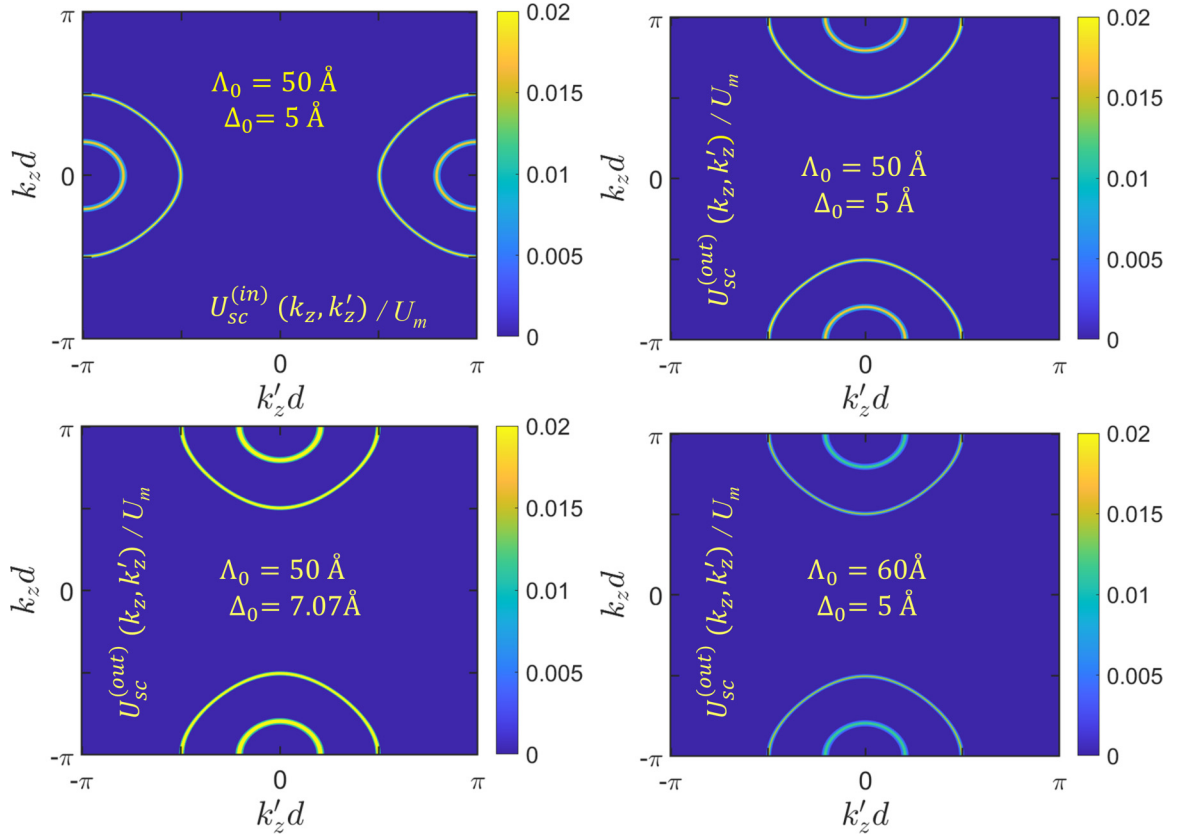
FIG. 2. Selected 2D density plots for numerically calculated effective quasi-1D static scattering potentials $U_{sc}^{(in)}(k_z, k_z')/U_m$ and $U_{sc}^{(out)}(k_z, k_z')/U_m$ as functions of wave numbers k_z and k_z' from Eqs. (16) and (17), respectively, with various combinations for values of Λ_0 and Δ_0 in four panels, where $T = T_0 = 4$ K is assumed and $U_m = 1$ eV is selected as a scale for calculated potentials.

With help from this determined chemical potential $\mu_0(T)$, we further acquire the initial quantum-well areal density n_{qw} of electrons, introduced in Eq. (25), simply by $n_{qw} \approx \rho_0 d$.

Finally, by applying the numerically computed transient non-equilibrium occupation function $\Delta n(k_z, t)$ from Eq. (9), the transient drift velocity $v_d(t; \mathcal{E}_0)$ for miniband electrons in a *SL* can be calculated from a quantum-statistical average of electron group velocity $v_z(k_z)$, [34] leading to

$$v_d(t; \mathcal{E}_0) = \frac{\sum_{k_z} v_z(k_z) \Delta n(k_z, t)}{\sum_{k_z} n_0(k_z)}$$

$$= \frac{\int_{-\pi/d}^{\pi/d} dk_z \, v_z(k_z) \, \Delta n(k_z, t)}{\int_{-\pi/d}^{\pi/d} dk_z \, n_0(k_z)}, \qquad (27)$$

where $v_z(k_z) = (\mathcal{W}_0 d/2\hbar) \sin(k_z d)$ is the group velocity of miniband electrons along a SL direction. Having obtained $v_d(t; \mathcal{E}_0)$, we can calculate the thermal dissipation power $\mathcal{P}(t; \mathcal{E}_0)$, given by

$$\mathcal{P}(t; \mathcal{E}_0) = \frac{v_d(t; \mathcal{E}_0) d}{2\pi} \int_{-\pi/d}^{\pi/d} dk_z \, f_{res}(k_z, t), \qquad (28)$$

which generates joule heating to a *SL* system. In addition, the DC vertical mobility $\mu(t; \mathcal{E}_0)$ can also be determined from $\mu(t; \mathcal{E}_0) = \partial v_d(t; \mathcal{E}_0)/\partial \mathcal{E}_0$, which depends on $\mathcal{E}_0$ due to nonlinear nature of electron transport or current [34]. Particularly, the transient current $I(t; \mathcal{E}_0)$ for the vertical transport of

electrons in SLs is found to be

$$I(t; \mathcal{E}_0) = \frac{-e}{\pi} \int_{-\pi/d}^{\pi/d} dk_z \, v_z(k_z) \, \Delta n(k_z, t)$$

$$= \frac{-e\mathcal{W}_0 d}{2\pi\hbar} \int_{-\pi/d}^{\pi/d} dk_z \, \sin(k_z d) \, \Delta n(k_z, t). \qquad (29)$$

TABLE I. Parameters used for numerical computations of vertical electron transport in GaAs/AlGaAs SLs unless they are indicated in figure captions.

| Parameter	Description	Value	Unit
Δ_0	Average interface roughness	5	Å
Λ_0	In-plane correlation length	50	Å
$\hbar\Omega_0$	Energy-level separation	100	meV
T_0	Temperature	4	K
$\hbar\Gamma_0$	Electron lifetime broadening	1	meV
m^*	In-plane electron effective mass	0.067	9.1×10^{-31} kg
d	SL period	100	Å
$2a$	Well width	40	Å
ρ_0	Electron volume density	1	10^{16} cm^{-3}
$\mathcal{E}_0$	DC electric field	500	V/cm
$\mathcal{W}_0$	Miniband width	10	meV
$N_0 + 1$	Number of *SL* periods	51	unit-less
M	Number of time steps	5	unit-less
Δt	Waiting time	10	ps
δ_0	Broadening time	0.5	ps
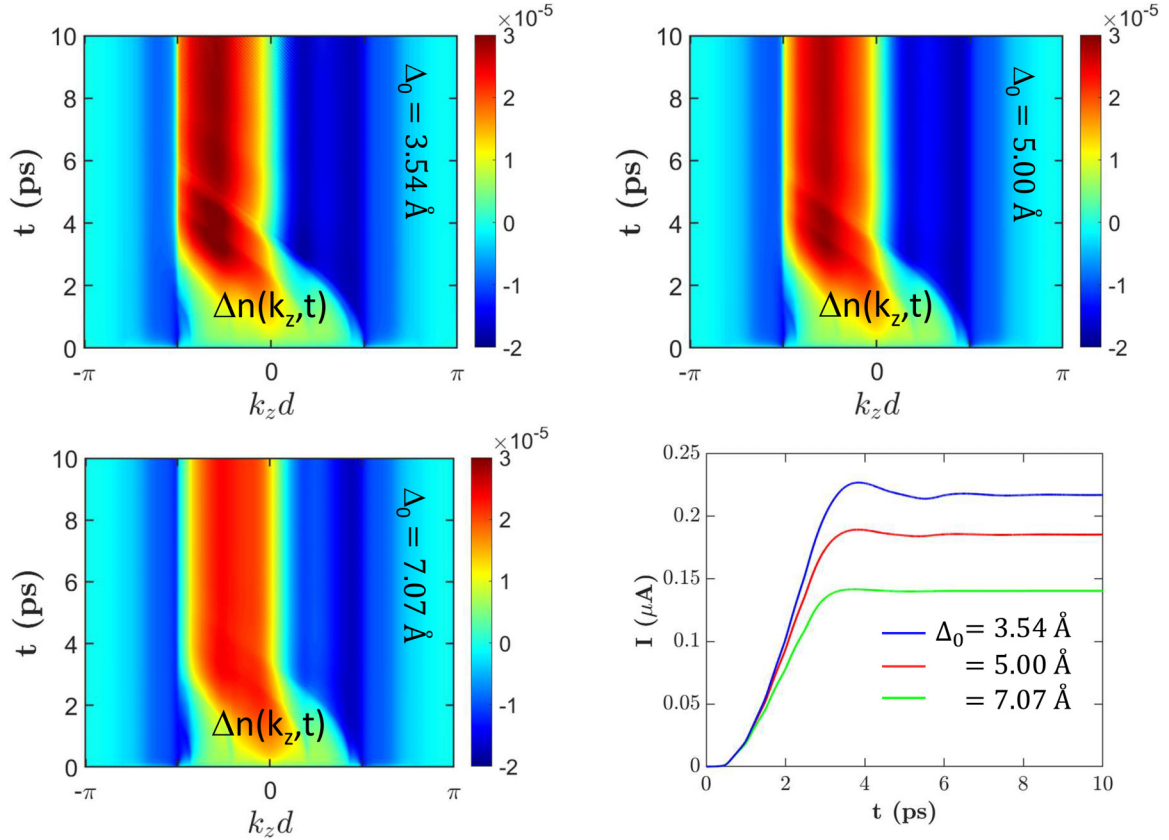
FIG. 3. 2D density plots for numerically calculated quasi-1D nonequilibrium occupation functions $\Delta n(k_z, t)$ from Boltzmann transport equation as functions of wave number k_z and time t with various values for $\Delta_0 = 3.54, 5.00, 7.07$ Å but fixed values of $\Lambda_0 = 50$ Å and $f_0 = 500$ eV/cm, as well as plot for corresponding transient currents $I(t; \mathcal{E}_0)$ as a function of time t with various values for Δ_0 in the bottom-right panel. Here, $T = T_0 = 4$ K is assumed.

Interestingly, if $f_{\text{res}}(t) = 0$ is taken and $|\Delta n(k_z, t)|$ is assumed small, the nonequilibrium occupation function $n(k_z, t)$ in steady states ($t \to \infty$) can be found after we linearize the 1D Boltzmann transport equation in Eq. (9) with respect to $\Delta n(k_z)$ for impurity [41], phonon [42], and Coulomb [38] scattering of electrons, respectively.

III. NUMERICAL RESULTS AND DISCUSSIONS

The used model parameters for all our numerical computations are listed in Table I. With the use of Eqs. (16) and (17), we present our numerically calculated effective quasi-1D scattering potentials $U_{\text{sc}}^{(\text{in})}(k_z, k_z')/U_m$ and $U_{\text{sc}}^{(\text{out})}(k_z, k_z')/U_m$ in Fig. 2 as functions of the wave numbers k_z and k_z' for both scattering-in and scattering-out processes, respectively. Due to the presence of an energy-conservation constraint for 3D elastic-scattering processes, both positive $U_{\text{sc}}^{(\text{in})}(k_z, k_z')/U_m$ and $U_{\text{sc}}^{(\text{out})}(k_z, k_z')/U_m$ appear significant only within two "curve-like" regions with mirror symmetry and vary their strengths dramatically with average interface roughness Δ_0 and in-plane correlation length Λ_0. This mirror symmetry displays a 90°-degree rotation as $U_{\text{sc}}^{(\text{in})}(k_z, k_z')/U_m$ switches to $U_{\text{sc}}^{(\text{out})}(k_z, k_z')/U_m$ and vice versa. Physically speaking, these quasi-1D scattering processes, as characterized by two effective scattering potentials $U_{\text{sc}}^{(\text{in})}(k_z, k_z')/U_m$ and $U_{\text{sc}}^{(\text{out})}(k_z, k_z')/U_m$ are inelastic ones in nature although

their corresponding 3D scattering processes still remain elastic. Quantitatively, we find both $U_{\text{sc}}^{(\text{in})}(k_z, k_z')/U_m$ and $U_{\text{sc}}^{(\text{out})}(k_z, k_z')/U_m$ goes up with increased Δ_0 but drops as Λ_0 becomes large.

By exactly solving the quasi-1D Boltzmann transport equation in Eq. (9) for the nonequilibrium occupation function $\Delta n(k_z, t)$ of drifting electrons in a SL beyond the well-known relaxation-time approximation, we display 2D density plots for numerically computed $\Delta n(k_z, t)$ in Fig. 3 at $T = T_0 = 4$ K with different values for the average interface roughness Δ_0, as well as a comparison of their corresponding currents $I(t; \mathcal{E}_0)$ as a function of time t. From Eq. (29), we know that $I(t; \mathcal{E}_0)$ should be determined only by the nonequilibrium part $\Delta n(k_z, t)$ of a full occupation function of electrons, instead of a full occupation function $n(k_z, t)$. For these cases with $\Lambda_0 = 50$ Å, $f_0 = 500$ eV/cm and various roughness parameters Δ_0, we find that $I(t; \mathcal{E}_0)$ decreases with increasing Δ_0 due to gradually enhanced interface-roughness scattering strength, as revealed by Eqs. (16) and (17). Under a strong electric force $f_0 = 500$ eV/cm, the strip-shaped $\Delta n(k_z, t)$ is pushed away with time from its initial symmetrical position around the Brillouin-zone center at $k_z = 0$ to the left-side asymmetrical $k_z < 0$ region, leading to a finite and positive current $I(t; \mathcal{E}_0)$, agreeing with the prediction from Eq. (29). Moreover, the central dark-color bar (maximum) inside this stripe-shaped region and near $k_z d = -\pi/2$ for a maximum absolute value of group
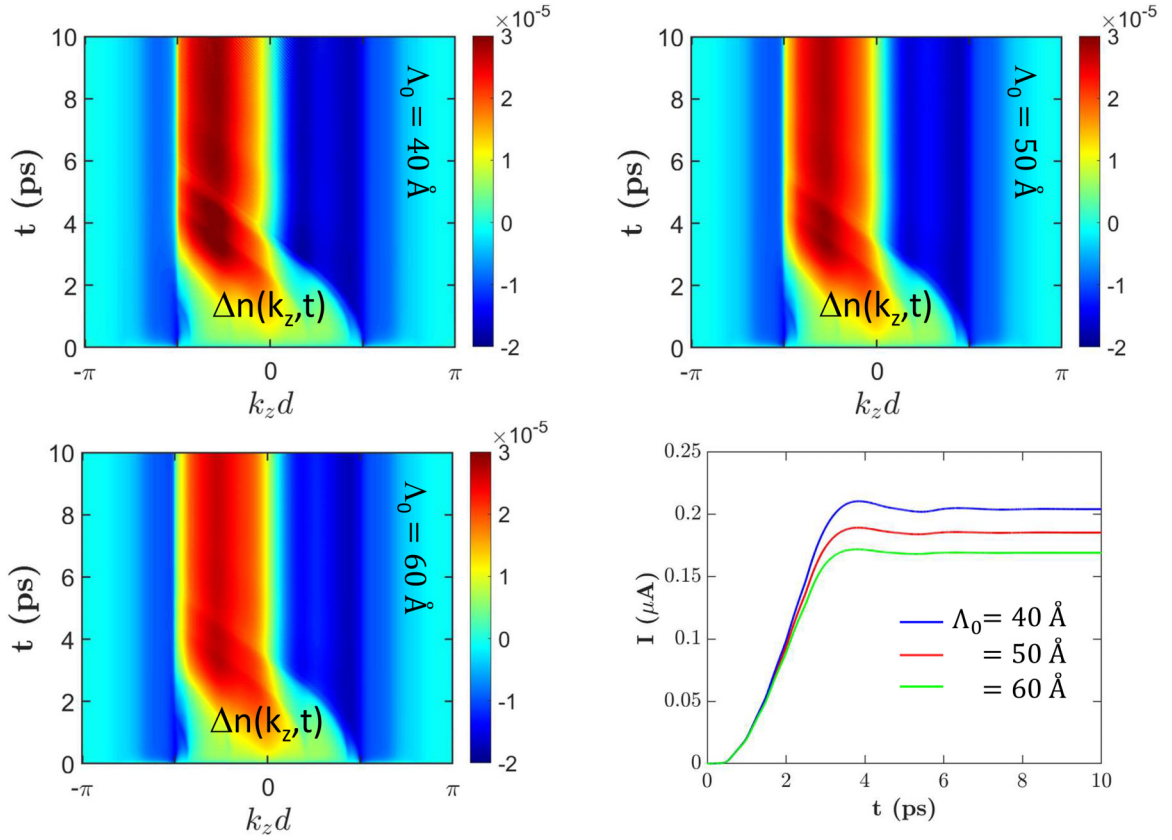
FIG. 4. 2D density plots for numerically calculated quasi-1D nonequilibrium occupation functions $\Delta n(k_z, t)$ from Boltzmann transport equation as functions of wave number k_z and time t with various values for $\Lambda_0 = 40, 50, 60\,\text{Å}$ but fixed values of $\Delta_0 = 5\,\text{Å}$ and $f_0 = 500\,\text{eV/cm}$, as well as plot for corresponding transient currents $I(t; \mathcal{E}_0)$ as a function of time t with various values for Λ_0 in the bottom-right panel. Here, $T = T_0 = 4\,\text{K}$ is assumed.

velocity has been smeared out quickly as Δ_0 is increased from $3.54\,\text{Å}$ to $7.07\,\text{Å}$, resulting in a reduced current $I(t; \mathcal{E}_0)$ with increasing Δ_0.

We now turn our attention to the effect due to the in-plane correlation length Λ_0 on the distribution of $\Delta n(k_z, t)$ in k_z-space, and on the magnitude change of $I(t; \mathcal{E}_0)$ as well. From Fig. 4, we see a similar feature from their dependence on in-plane correlation length parameter Λ_0 (characterizing the area density of interface roughness) in comparison with those from their dependence on average interface-roughness amplitude Δ_0 in Fig. 3, where $I(t; \mathcal{E}_0)$ increases with reducing value of Λ_0. In fact, as revealed by Eqs. (16) and (17), $I(t; \mathcal{E}_0)$ depends on Λ_0 through an exponential factor of $\sim \Lambda_0^2 \exp[-\mathcal{P}_0(k_\parallel, k'_\parallel, \theta_0)\Lambda_0^2/4]$, which is slightly different from its dependence on Δ_0 in Fig. 3 through a proportional factor of $\sim \Delta_0^2$. Practically, however, both Δ_0 and Λ_0 can be attributed to and determined by a particular sample-growth process.

Since the presence of an electric current $I(t; \mathcal{E}_0)$ is always subjected to an applied electric force f_0 or a DC electric field $\mathcal{E}_0$ experimentally, we study such a case in Fig. 5 by displaying 2D density plots for $\Delta n(k_z, t)$ as functions of time t and wave number k_z of electrons under different strengths of f_0 in Fig. 5, ranging from $50\,\text{eV/cm}$ up to $500\,\text{eV/cm}$. From Fig. 5, one easily visualizes a full physical mechanism and process for producing a conduction current flowing through a SL structure. Such a process starts

from continuously shifting a nonequilibrium part $\Delta n(k_z, t)$ of electron occupation function towards negative k_z direction with an increasing electric force f_0 until $k_z d = -\pi/2$ is reached, which is accompanied by an enhanced conduction current $I(t; \mathcal{E}_0)$ at the same time. When $f_0 = 500\,\text{eV/cm}$, a central dark-color bar close to $k_z d = -\pi/2$ occurs inside the stripe-shaped region, which greatly increases the conduction current $I(t; \mathcal{E}_0)$ in this case. The fact that the shift of $\Delta n(k_z, t)$ towards negative k_z direction with increasing f_0 is blocked at $k_z d = -\pi/2$ demonstrates a so-called "negative effective mass" $m^*(k_z)$ determined by $1/m^*(k_z) = (1/\hbar^2)\, d^2 E_z(k_z)/dk_z^2 = (\mathcal{W}_0 d^2/2\hbar^2)\cos(k_z d)$, [46,47] which becomes negative in the range of $-\pi < k_z d < -\pi/2$.

For the purpose of displaying an easy-reading comparison, we first put together numerically computed $I(t; \mathcal{E}_0)$ for its dependence on Δ_0, Λ_0 and f_0, respectively, in three upper panels of Fig. 6, which were already presented in Figs. 3–5, separately. Importantly, the extracted steady-state currents at the final time $t = 10\,\text{ps}$ are exhibited simultaneously, in the three lower panels of Fig. 6. Here, under a relatively strong DC electric force at $f_0 = 500\,\text{eV/cm}$, both variations of $I(t; \mathcal{E}_0)$ with respect to average interface-roughness amplitude Δ_0 and to in-plane correlation length Λ_0 appear linearly and look similar to each other qualitatively. However, the dependence of $I(t; \mathcal{E}_0)$ on an electric force f_0, or a DC electric field $\mathcal{E}_0$, presents a quite unique nonlinear feature. This nonlinear dependence implies that the electric conductivity
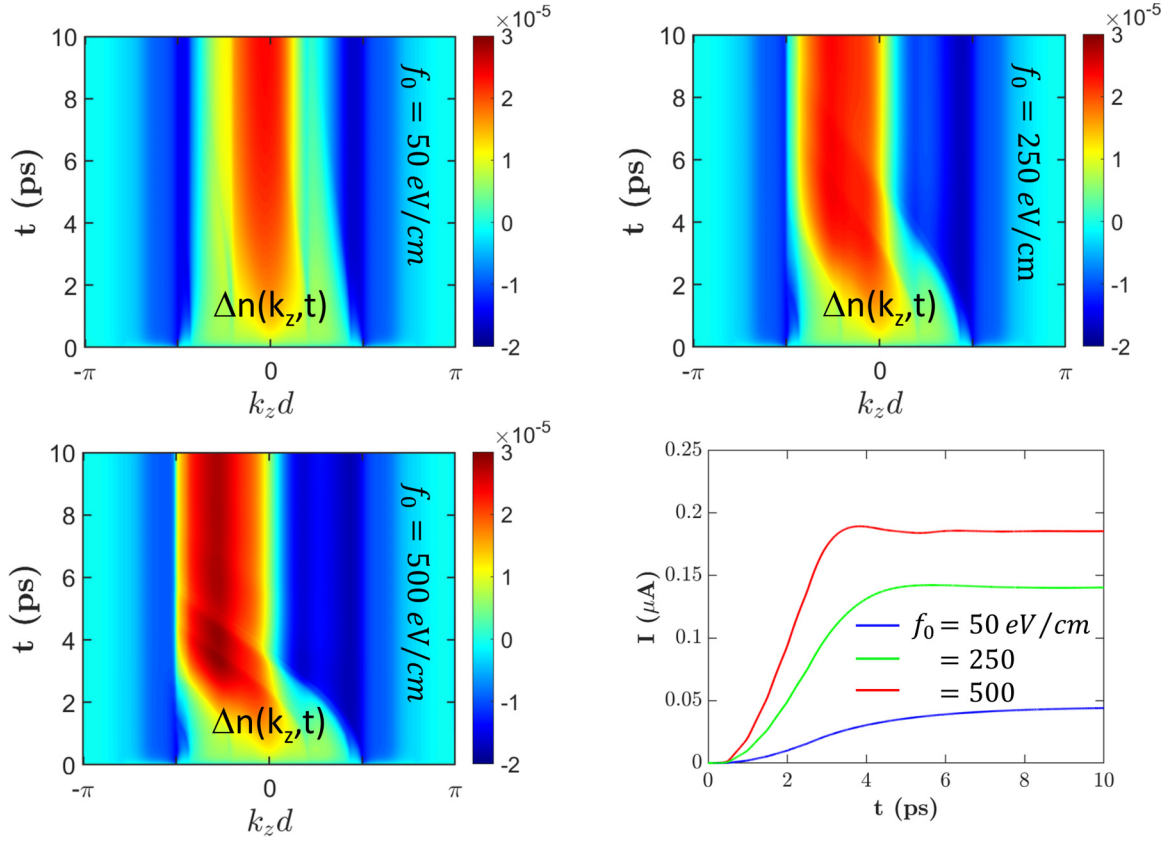
FIG. 5. 2D density plots for numerically calculated quasi-1D nonequilibrium occupation functions $\Delta n(k_z, t)$ from Boltzmann transport equation as functions of wave number k_z and time t with various values for $f_0 = 50, 250, 500\,\text{eV/cm}$ but fixed values of $\Delta_0 = 5\,\text{Å}$ and $\Lambda_0 = 50\,\text{Å}$, as well as plot for corresponding transient currents $I(t; \mathcal{E}_0)$ as a function of time t with various values for f_0 in the bottom-right panel. Here, $T = T_0 = 4\,\text{K}$ is assumed.
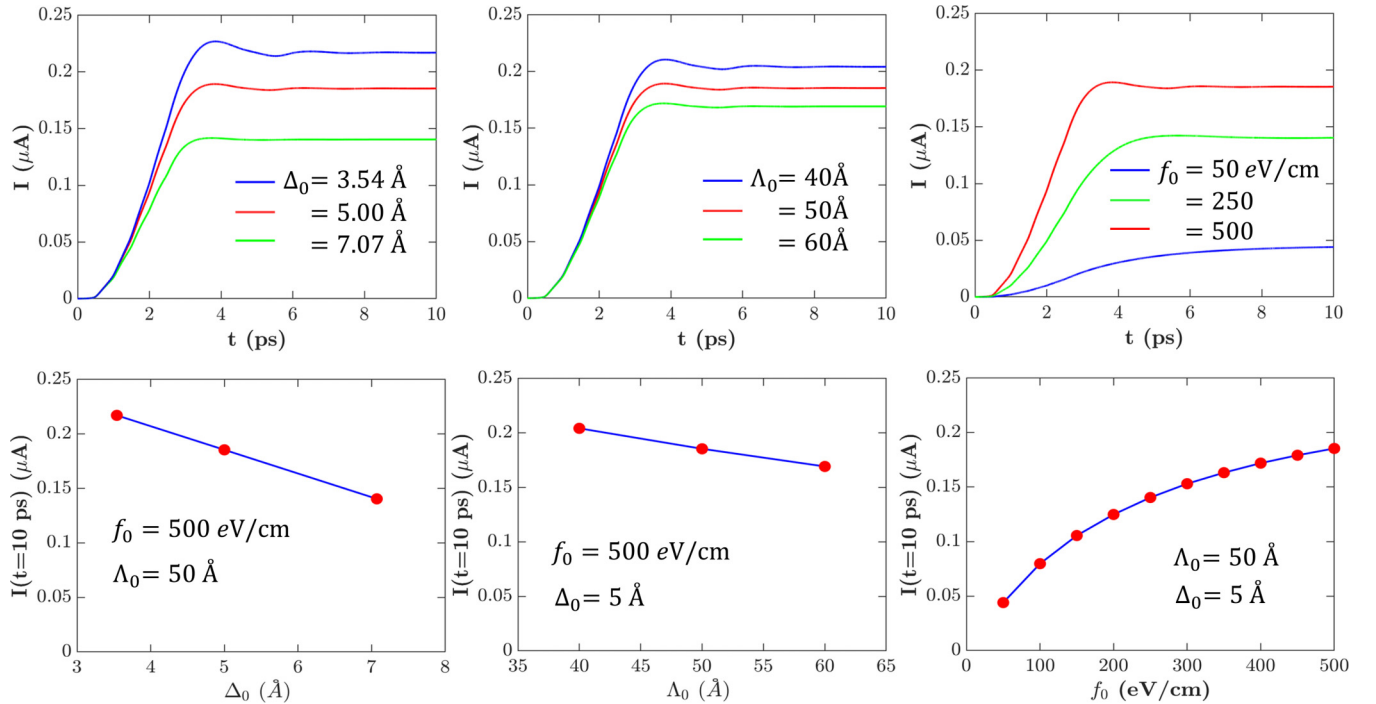
FIG. 6. (Upper) Numerically calculated transient currents $I(t; \mathcal{E}_0)$ as a function of time t with various values for $\Delta_0 = 3.54, 5.00, 7.07\,\text{Å}$ (left), $\Lambda_0 = 40, 50, 60\,\text{Å}$ (middle), and $f_0 = 50, 250, 500\,\text{eV/cm}$ (right). (Lower) Numerically calculated steady-state currents I at $t = 10\,\text{ps}$ as a function of Δ_0 for $\Lambda_0 = 50\,\text{Å}$ and $f_0 = 500\,\text{eV/cm}$ (left), a function of Λ_0 for $\Delta_0 = 5\,\text{Å}$ and $f_0 = 500\,\text{eV/cm}$ (middle), as well as a function of f_0 for $\Delta_0 = 5\,\text{Å}$ and $\Lambda_0 = 50\,\text{Å}$ (right). Here, $T = T_0 = 4\,\text{K}$ is assumed.
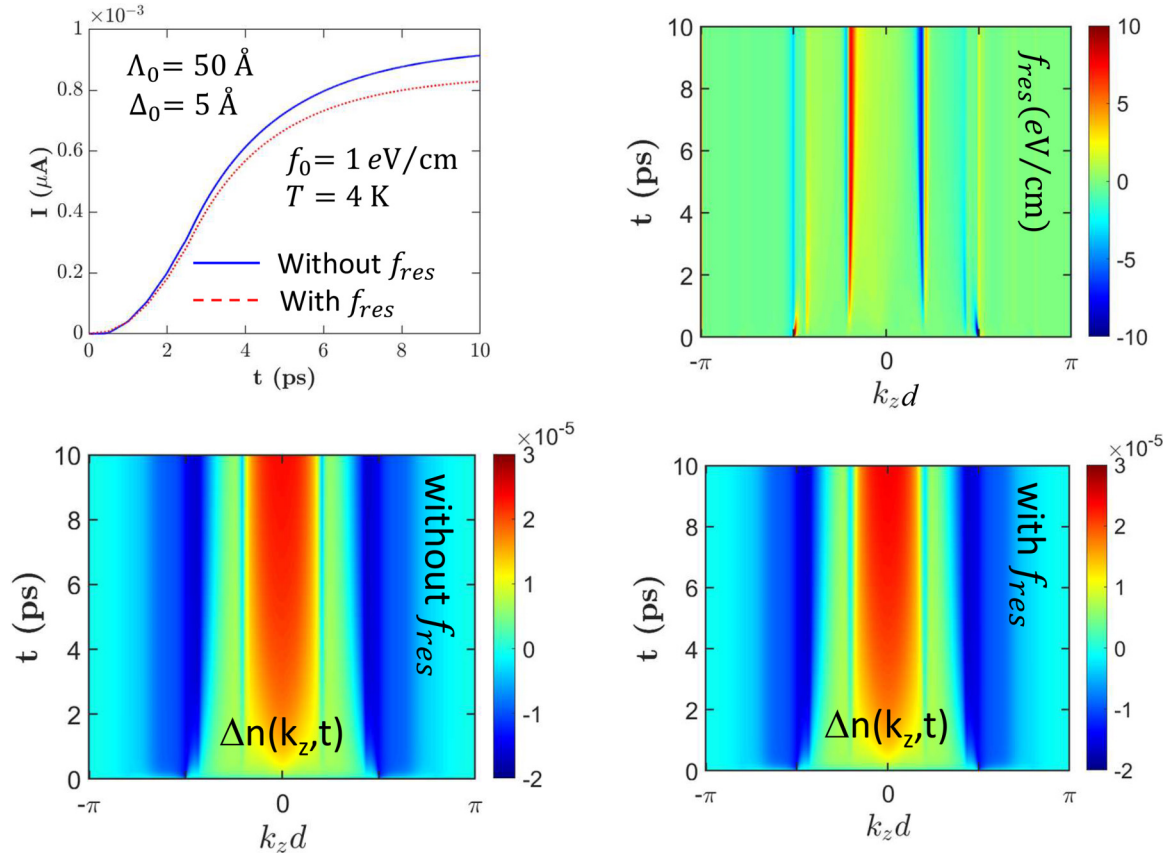
FIG. 7. (Upper) Numerically calculated transient currents $I(t; \mathcal{E}_0)$ with (dashed curve) and without (solid curve) inclusion of a dynamical scattering force $f_{res}(k_z, t)$ as a function of time t under $\Delta_0 = 5$ Å, $\Lambda_0 = 50$ Å, and $f_0 = 1$ eV/cm (left), as well as 2D density plots for a dynamical scattering force $f_{res}(k_z, t)$ as functions of wave number k_z and time t (right) for the same parameters used in the left panel. (Lower) 2D density plots for numerically calculated quasi-1D nonequilibrium occupation functions $\Delta n(k_z, t)$ from Boltzmann transport equation as functions of wave number k_z and time t with (right) and without (left) inclusion of $f_{res}(k_z, t)$ for the same parameters employed in upper panels. Here, $T = T_0 = 4$ K is assumed.

$\propto \partial I(t; \mathcal{E}_0)/\partial \mathcal{E}_0$ is no longer a constant and appears as a decreasing function of the applied field $\mathcal{E}_0$ instead, i.e., a non-ohmic behavior.

Physically, as predicted by Eq. (18), besides an external electric force f_0, there exists another internal scattering force $f_{res}(k_z, t)$, which depends on the electronic state through the wave number k_z, as well as on time t dynamically. Such an internal scattering force $f_{res}(k_z, t)$ should be determined self-consistently based on Eqs. (19) to (24) and taken into consideration for our generalized Boltzmann transport equation in Eq. (9). To reveal the dynamical nature and significance of $f_{res}(k_z, t)$, we show in Fig. 7 a comparison of computed conduction currents $I(t; \mathcal{E}_0)$ either with (dashed curve) or without (solid curve) inclusion of this scattering force $f_{res}(k_z, t)$. From this figure, we observe that both positive and negative $f_{res}(k_z, t)$ become significant only at two boundaries $k_z d = \pm\pi/2$ of a nonshifted strip-shaped region because of its dominant dependence on $\partial \Delta n(k_z, t)/\partial k_z$ in Eq. (24). Interestingly, for a very weak electric force $f_0 = 1$ eV/cm utilized in Fig. 7, the condition for $f_{res}(k_z, t) > |f_0|$ can be satisfied, implying the direction of a total force in the generalized Boltzmann transport equation can be reversed for some electronic states with a specific wave number k_z although the overall driving effect for SL electrons still remains in the $-k_z$ direction. Such

a force-direction switching can produce a visible reduction of conduction current $I(t; \mathcal{E}_0)$ for a weak external electric force $f_0 = 1$ eV/cm, as demonstrated in this figure.

As the electric force f_0 is increased to 500 eV/cm in Fig. 8, the maximum of the scattering force $f_{res}(k_z, t)$ also reaches 20 eV/cm, which is, however, still much smaller than f_0 in this case. Therefore, we do not expect the occurrence of a reversed direction for a total electric force acting on electrons as in Fig. 7. Therefore, there is no visible difference between conduction currents $I(t; \mathcal{E}_0)$ with (dashed curve) and without (solid curve) inclusion of a dynamical scattering force $f_{res}(k_z, t)$ as a function of time t under $\Delta_0 = 5$ Å, $\Lambda_0 = 50$ Å, and $f_0 = 500$ eV/cm at a very low temperature $T = T_0 = 4$ K. Moreover, the internal scattering force $f_{res}(k_z, t)$ as a function of electron wave number k_z is found significant only around $k_z d = -\pi/2$ in this case, and consequently, no visible change in conduction current $I(t; \mathcal{E}_0)$ becomes visible.

As the temperature T is lifted up from $T_0 = 4$ K to $T_0 = 77$ K in Fig. 9, the resulting conduction current $I(t; \mathcal{E}_0)$ is reduced dramatically by one order of magnitude for the same parameters used in Fig. 8. In fact, for a raised temperature T from 4 K to 77 K, the introduced in-plane thermal-equilibrium Fermi function $f_0[E_{xy}(k_\parallel) - \mu_0]$ of electrons in Eqs. (16) and (17) will be reduced in magnitude around $k_\parallel = 0$ whereas it is
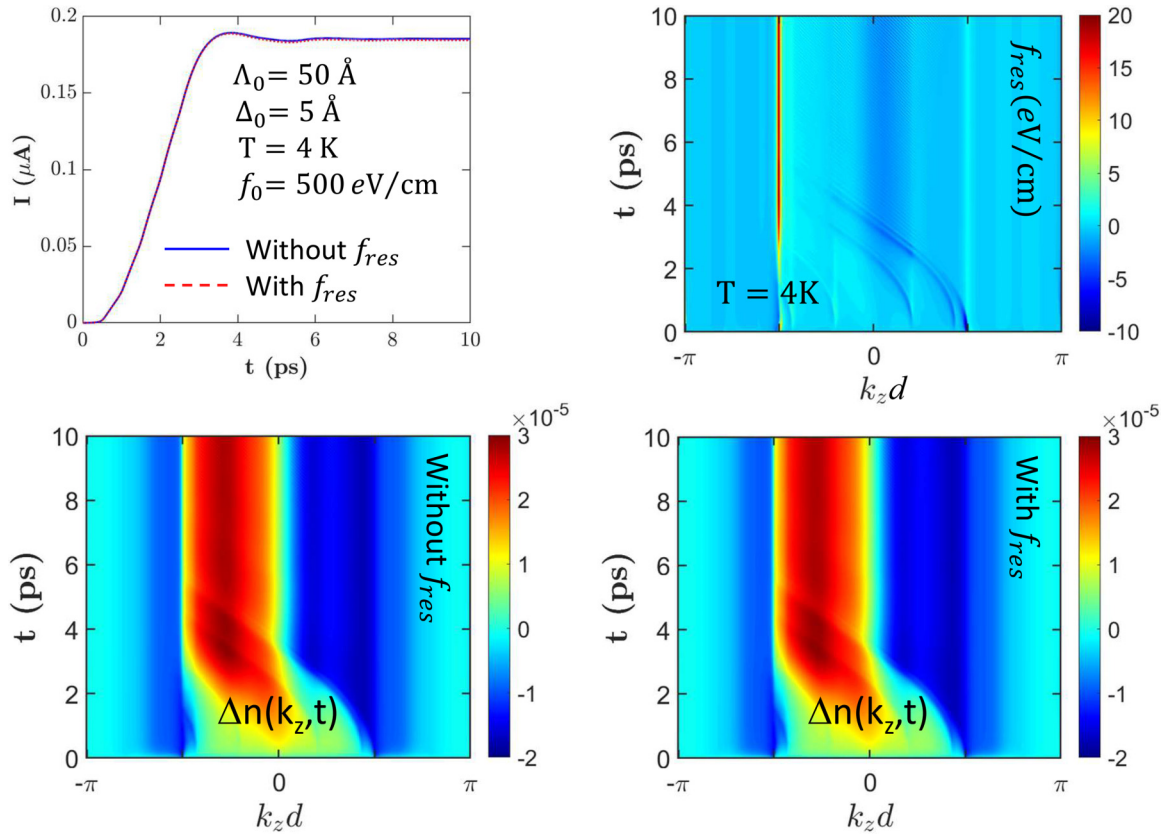
FIG. 8. (Upper) Numerically calculated transient currents $I(t; \mathcal{E}_0)$ with (dashed curve) and without (solid curve) inclusion of a dynamical scattering force $f_{\mathrm{res}}(k_z, t)$ as a function of time t under $\Delta_0 = 5\,\text{Å}$, $\Lambda_0 = 50\,\text{Å}$, and $f_0 = 500\,\text{eV/cm}$ (left), as well as 2D density plots for a dynamical scattering force $f_{\mathrm{res}}(k_z, t)$ as functions of wave number k_z and time t (right) for the same parameters used in the left panel. (Lower) 2D density plots for numerically calculated quasi-1D non-equilibrium occupation functions $\Delta n(k_z, t)$ from Boltzmann transport equation as functions of wave number k_z and time t with (right) and without (left) inclusion of $f_{\mathrm{res}}(k_z, t)$ for the same parameters employed in upper panels. Here, $T = T_0 = 4\,\text{K}$ is assumed.

increased beyond the low-T occupation boundary at $k = k_F$, where k_F represents the Fermi wave number for free electrons in 2D $\boldsymbol{k}_\parallel$-space. As a result, electrons in large $\boldsymbol{k}_\parallel$ states will contribute to in-plane roughness scattering processes as predicted by Eqs. (16) and (17). This greatly decreases the vertical conduction current $I(t; \mathcal{E}_0)$, as displayed in Fig. 9. Compared with the nonequilibrium part $\Delta n(k_z, t)$ of electron occupation function presented in Fig. 8, it is decreased by about one order of magnitude in Fig. 9. Meanwhile, both boundaries of a shifted strip-shaped region are softened significantly by thermal effects at a higher temperature $T = T_0 = 77\,\text{K}$, and furthermore, the central dark-color bar near $k_z d = -\pi/2$ inside the stripe-shaped region has been washed away completely. Finally, we also notice from Fig. 9 that the internal scattering force $f_{\mathrm{res}}(k_z, t)$ drops by one order of magnitude due to thermal effects at an elevated temperature $T = T_0 = 77\,\text{K}$.

IV. CONCLUSION AND REMARKS

In conclusion, we proposed an effective scattering-potential approach for treating interface-roughness scattering of field-driven miniband electrons within a type-I semiconductor superlattice structure. Based on these calculated effective scattering potentials, we further introduced a generalized

Boltzmann transport equation by including self-consistently an internal scattering force which is time-dependent and electronic-state specific. Meanwhile, we solved exactly this generalized Boltzmann transport equation by going beyond the commonly used relaxation-time approximation.

As an exact solution to the generalized Boltzmann transport equation, we analyzed the dependence of our numerically computed nonequilibrium electron occupation function on different interface-roughness parameters. Using this obtained solution under a strong DC electric field, we revealed some unique features in reduced conduction current with respect to in-plane correlation length and average interface-roughness amplitude at various temperatures and DC electric-field strengths. More importantly, on a microscopic level, we enabled quantitatively visualizing physical mechanism associated with nonlinear transport of miniband electrons or non-ohmic behavior as demonstrated by our numerical results.

From a mathematical point of view, the proposed effective scattering-potential approach presented in this paper can be utilized for treating other types of electron scattering, such as impurity, phonon and electron-electron scattering if they are mostly limited to a 2D wave-vector space. Technically, on the other hand, the currently performed numerical investigation on vertical transport in type-I superlattices can be generalized
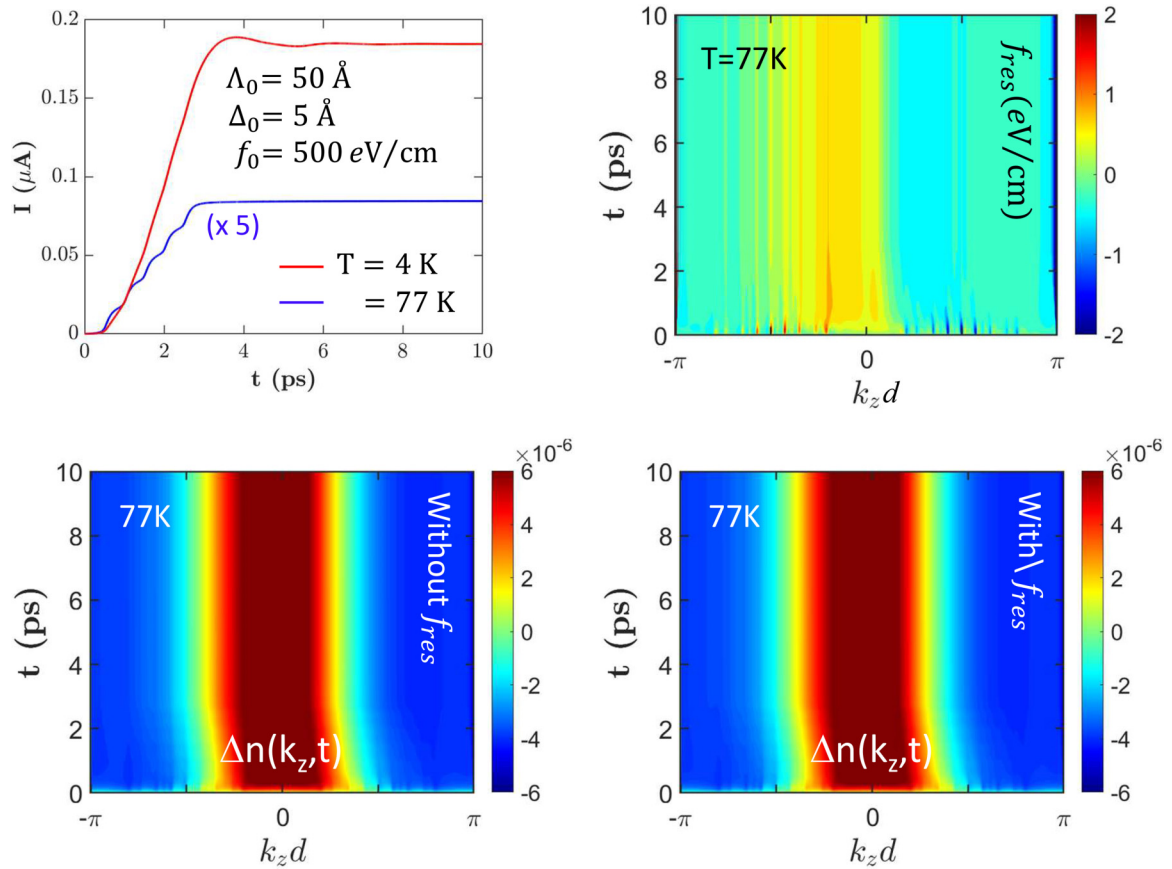
FIG. 9. (Upper) Numerically calculated transient currents $I(t; \mathcal{E}_0)$ with (dashed curve) and without (solid curve) inclusion of a dynamical scattering force $f_{res}(k_z, t)$ as a function of time t under $\Delta_0 = 5$ Å, $\Lambda_0 = 50$ Å, and $f_0 = 500$ eV/cm (left), as well as 2D density plots for a dynamical scattering force $f_{res}(k_z, t)$ as functions of wave number k_z and time t (right) for the same parameters used in the left panel. (Lower) 2D density plots for numerically calculated quasi-1D non-equilibrium occupation functions $\Delta n(k_z, t)$ from Boltzmann transport equation as functions of wave number k_z and time t with (right) and without (left) inclusion of $f_{res}(k_z, t)$ for the same parameters employed in upper panels. Here, $T = T_0 = 77$ K is assumed. The label $\times 5$ in upper left panel indicates the scale of blue solid curve has been amplified by a factor of 5 for $T = T_0 = 77$ K.

to type-II superlattice structures under a tilted nonquantizing magnetic field and utilized for third-generation infrared focal-plane arrays and photodiodes.

In a general case as formulated in this paper, we require a 3D elastic scattering model when electrons are driven perpendicularly. Therefore, one deals with a six-dimensional phase space for initial- and final-state scattering wave vectors, q and q', of an electron in numerical computations. Due to total-energy conservation for a scattering electron, this reduces the previous dimensionality of phase space from six to five. If a 3D electron-electron coulomb scattering is considered, the reduced dimensionality of the system will be eight, by taking into account the conservation of total momentum and energy for the scattering between a pair of electrons.

By going beyond our currently proposed quasi-1D time-dependent theory, a full theory for the same system considered in this paper requires an accurate description for 2D parallel interface-roughness scattering of driven electrons along the vertical SL direction. Therefore, a 3D scattering model, instead of a 2D scattering model, is mandated for studying scattering dynamics of electrons in such a system. If electrons

are driven within the scattering plane, however, only a 2D scattering model is needed for such a case.

In our current quantum-kinetic model, the in-plane roughness scattering of electrons is assumed remaining in a thermal-equilibrium state with a constant initial temperature T_0 within a 2D $q_\parallel$-phase space. The criteria for the presence of such an in-plane thermal-equilibrium occupation function is give by $e\mathcal{E}_0 d/\hbar v_d > 1/\Lambda_0$. However, the partial occupation function $n(k_z, t)$ of electrons in the q_z-phase space, which leads to an electron transport under a DC electric field, becomes a nonequilibrium and nonthermal one. Therefore, an initial thermal-equilibrium temperature T_0 can only be used for in-plane thermal-equilibrium scattering electrons but cannot be employed for driving electrons along the superlattice direction. Instead, one should introduce an effective temperature T_{eff}, which is defined as the change of average kinetic energy of electrons along the superlattice direction in their nonequilibrium and nonthermal states. In the presence of a strong DC electric field, one finds T_{eff} becomes larger than T_0 in this system, leading to a dramatic field-induced electron heating [34].

[1] A. Rogalski and P. Martyniuk, InAs/GaInSb superlattices as a promising material system for third generation infrared detectors, Infrared Phys. Technol. **48**, 39 (2006); A. Rogalski, J. Antoszewski, and L. Faraone, Third-generation infrared photodetector arrays, J. Appl. Phys. **105**, 091101 (2009).

[2] Q. K. Yang, F. Fuchs, J. Schmitz, and W. Pletschen, Investigation of trap-assisted tunneling current in InAs/(GaIn)Sb superlattice long-wavelength photodiodes, Appl. Phys. Lett. **81**, 4757 (2002).

[3] R. Rehm, M. Walther, F. Fuchs, J. Schmitz, and J. H. Fleissner, Passivation of InAs/(GaIn)Sb short-period superlattice photodiodes with 10 μm cutoff wavelength by epitaxial overgrowth with $Al_xGa_{1-x}As_ySb_{1-y}$, Appl. Phys. Lett. **86**, 173501 (2005).

[4] B.-M. Nguyen, D. Hoffman, E. K.-W. Huang, P.-Y. Delaunay, and M. Razeghi, Background limited long wavelength infrared type-II InAs/GaSb superlattice photodiodes operating at 110K, Appl. Phys. Lett. **93**, 123502 (2008); S. A. Pour, E. K. Huang, G. Chen, A. Haddadi, B.-M. Nguyen, and M. Razeghi, High operating temperature midwave infrared photodiodes and focal plane arrays based on type-II InAs/GaSb superlattices, *ibid.* **98**, 143501 (2011).

[5] A. Hood, M. Razeghi, E. H. Aifer, and G. J. Brown, On the performance and surface passivation of type II InAs/GaSb superlattice photodiodes for the very-long-wavelength infrared, Appl. Phys. Lett. **87**, 151113 (2005).

[6] H. J. Haugan, F. Szmulowicz, K. Mahalingam, G. J. Brown, S. R. Munshi, and B. Ullrich, Short-period InAs/GaSb type-II superlattices for mid-infrared detectors, Appl. Phys. Lett. **87**, 261106 (2005).

[7] F. Szmulowicz, H. J. Haugan, G. J. Brown, K. Mahalingam, B. Ullrich, S. R. Munshi, and L. Grazulis, Interfaces as design tools for short-period InAs/GaSb type-II superlattices for mid-infrared detectors, Opto-Electronics Rev. **14**, 69 (2006).

[8] E. Plis, J. B. Rodriguez, G. Balakrishnan, Y. D. Sharma, H. S. Kim, T. Rotter, and S. Krishna, Mid-infrared InAs/GaSb strained layer superlattice detectors with nBn design grown on a GaAs substrate, Semicond. Sci. Technol. **25**, 085010 (2010).

[9] W. W. Bewley, J. R. Lindle, C. S. Kim, M. Kim, C. L. Canedy, I. Vurgaftman, and J. R. Meyer, Lifetimes and Auger coefficients in type-II *W* interband cascade lasers, Appl. Phys. Lett. **93**, 041118 (2008).

[10] J. B. Rodriguez, C. Cervera, and P. Christol, A type-II superlattice period with a modified InAs to GaSb thickness ratio for midwavelength infrared photodiode performance improvement, Appl. Phys. Lett. **97**, 251113 (2010).

[11] N. Yoon, C. J. Reyner, G. Ariyawansa, J. M. Duran, J. E. Scheihing, J. Mabon, and D. Wasserman, Modified electron beam induced current technique for in(Ga)As/InAsSb superlattice infrared detectors, J. Appl. Phys. **122**, 074503 (2017).

[12] F. Aristone, J.-C. Portal, J. F. Palmier, and J. C. Harmand, Shubnikov–de Haas–like oscillations in the vertical transport of semiconductor superlattices, Braz. J. Phys. **29**, 375 (1999).

[13] A. Sibille, J. F. Palmier, H. Wang, and F. Mollot, Observation of Esaki-Tsu negative differential velocity in GaAs/AlAs superlattices, Phys. Rev. Lett. **64**, 52 (1990).

[14] F. Aristone, P. Gassot, J. F. Palmier, D. K. Maude, B. Goutiers, J. L. Gauffier, J. C. Portal, and G. Mollot, Probing the interface fluctuations in semiconductor superlattices using a magneto-transport technique, Superlattices Microstruct. **15**, 225 (1994).

[15] G. A. Umana-Membreno, H. Kala, J. Antoszewski, J. M. Dell, L. Faraone, B. Klein, G. Gautam, M. N. Kutty, E. Plis, and S. Krishna, Vertical transport in InAs/GaSb type-II strained layer superlattices for infrared focal plane array applications, Proc. SPIE **8012**, 80120Y (2011).

[16] L. Bürkle, F. Fuchs, R. Kiefer, W. Pletschen, R. E. Sah, and J. Schmits, Electrical characterization of InAs/(GaIn)Sb infrared superlattice photodiodes for the 8 to 12 νm range, MRS Online Proceedings Library **607**, 75 (1999).

[17] L. K. Casias, C. P. Morath, E. H. Steenbergen, G. A. Umana-Membreno, P. T. Webster, J. V. Logan, J. K. Kim, G. Balakrishnan, L. Faraone, and S. Krishna, Vertical carrier transport in strain-balanced InAs/InAsSb type-II superlattice material, Appl. Phys. Lett. **116**, 182109 (2020).

[18] R. W. Prange and T. W. Nee, Quantum spectroscopy of the low-field oscillations in the surface impedance, Phys. Rev. **168**, 779 (1968); H. Sakaki, T. Noda, K. Hirakawa, M. Tanaka, and T. Matsusue, Interface roughness scattering in GaAs/AlAs quantum wells, Appl. Phys. Lett. **51**, 1934 (1987); T. Noda, M. Tanaka, and H. Sakaki, Correlation length of interface roughness and its enhancement in molecular beam epitaxy grown GaAs/AlAs quantum wells studied by mobility measurement, *ibid.* **57**, 1651 (1990); U. Penner, H. Rücker, and I. N. Yassievich, Theory of interface roughness scattering in quantum wells, Semicond. Sci. Technol. **13**, 709 (1998); N. Balkan, R. Gupta, M. Cankurtaran, H. Celik, A. Bayrakli, E. Tiras, and M. C. Arikan, Well-width dependence of interface roughness scattering in GaAs/$Ga_{1-x}Al_x$As quantum wells, Superlattices Microstruct. **22**, 263 (1997); R. Nag, S. Mukyopadhyay, and M. Das, Interface roughness scattering-limited electron mobility in AlAs/GaAs and $Ga_{0.5}In_{0.5}$P/GaAs wells, J. Appl. Phys. **86**, 459 (1999); J. M. Li, J. J. Wu, X. X. Han, Y. W. Lu, X. L. Liu, Q. S. Zhu, and Z. G. Wang, A model for scattering due to interface roughness in finite quantum wells, Semicond. Sci. Technol. **20**, 1207 (2005); B. R. Nag, Interface roughness scattering limited mobility in AlAs/GaAs, $Al_{0.3}Ga_{0.7}$As/GaAs and $Ga_{0.5}In_{0.5}$P/GaAs quantum wells, *ibid.* **19**, 162 (2004); A. Gold, Interface-roughness parameters in InAs quantum

wells determined from mobility, J. Appl. Phys. **103**, 043718 (2008).

[19] F. Szmulowicz and G. J. Brown, Calculation of the vertical and horizontal electron mobilities in InAs/GaSb superlattices, Appl. Phys. Lett. **98**, 182105 (2011); Vertical transport in InAs/GaSb superlattices: model results and relation to in-plane transport, Proc. SPIE **7945**, 79451U (2011).

[20] S. Mori and T. Ando, Electronic properties of a semiconductor superlattice II. Low temperature mobility perpendicular to the superlattice, J. Phys. Soc. Jpn. **48**, 865 (1980).

[21] I. Dharssi and P. N. Butcher, The effect of phonon confinement on perpendicular electron transport in a GaAs/GaAlAs superlattice, J. Phys.: Condens. Matter **2**, 119 (1990).

[22] J. Q. You, L. Zhang, and Q. B. Yang, Longitudinal magneto-transport in long-period semiconductor superlattices, Phys. Rev. B **55**, 15757 (1997); G. J. Warren and P. N. Butcher, A mobility calculation for a GaAs/GaAlAs superlattice, Semicond. Sci. Technol. **1**, 133 (1986).

[23] G. Etemadi and J. F. Palmier, Effect of interface roughness on non-linear vertical transport in GaAs/AlAs superlattices, Solid State Commun. **86**, 739 (1993).

[24] J. R. Meyer, D. J. Arnold, C. A. Hoffman, F. J. Bartoli, and L. R. Ram-Mohan, Electron and hole in-plane mobilities in HgTe-CdTe superlattices, Phys. Rev. B **46**, 4139 (1992); C. A. Hoffman, J. R. Meyer, E. R. Youngdale, F. J. Bartoli, R. H. Miles, and L. R. Ram-Mohan, Electron transport in InAs/Ga$_{1-x}$In$_x$Sb superlattices, Solid-State Electron. **37**, 1203 (1994); Y. A. Pusep, G. C. Gozzo, and R. R. LaPierre, Interface roughness in short-period InGaAs/InP superlattices, Appl. Phys. Lett. **93**, 242104 (2008); T. V. Chandrasekhar Rao, J. Antoszewski, L. Faraone, J. B. Rodriguez, E. Plis, and S. Krishna, Characterization of carriers in GaSb/InAs superlattice grown on conductive GaSb substrate, *ibid.* **92**, 012121 (2008); C. Cervera, J. B. Rodrigue, J. P. Perez, H. Ait-Kaci, R. Chaghi, L. Konczewicz, S. Contreras, and P. Christol, Unambiguous determination of carrier concentration and mobility for InAs/GaSb superlattice photodiode optimization, J. Appl. Phys. **106**, 033709 (2009).

[25] F. Szmulowicz, H. J. Haugan, S. Elhamri, and G. J. Brown, Calculation of vertical and horizontal mobilities in InAs/GaSb superlattices, Phys. Rev. B **84**, 155307 (2011).

[26] L. Esaki and R. Tsu, Superlattice and negative differential conductivity in semiconductors, IBM J. Res. Dev. **14**, 61 (1970).

[27] H.-B. Lin, H. Zhong, N. Karpowicz, Y. Chen, and X.-C. Zhang, Terahertz spectroscopy and imaging for defense and security applications, Proc. IEEE **95**, 1514 (2007).

[28] D. Suqing, W. Zhang, and X.-G. Zhao, Current response of two-band superlattices at finite temperatures, Phys. Rev. B **62**, 9943 (2000).

[29] Z.-G. Wang, D. Suqing, and X.-G. Zhao, Photon-assisted transport and dynamical localization of semiconductor superlattices under a dc bichromatic electric field, Phys. Rev. B **69**, 035305 (2004).

[30] D. H. Dunlap and V. M. Kenkre, Dynamic localization of a charged particle moving under the influence of an electric field, Phys. Rev. B **34**, 3625 (1986).

[31] V. I. Puller, N. J. M. Horing, L. G. Mourokh, and A. Yu. Smirnov, Wave packet dynamics in a semiconductor superlattice, Phys. Lett. A **281**, 70 (2001).

[32] M. M. Dignam and C. M. de Sterke, Conditions for dynamic localization in generalized ac electric fields, Phys. Rev. Lett. **88**, 046806 (2002).

[33] M. J. Zhu, X.-G. Zhao, and Q. Niu, Manipulation of band electrons with a rectangular-wave electric field, J. Phys.: Condens. Matter **11**, 4527 (1999).

[34] J. R. Gulley and D. H. Huang, Self-consistent quantum-kinetic theory for interplay between pulsed-laser excitation and nonlinear carrier transport in a quantum-wire array, Opt. Express **27**, 17154 (2019).

[35] D. H. Huang, S. K. Lyo, and G. Gumbs, Bloch oscillation, dynamical localization, and optical probing of electron gases in quantum-dot superlattices in high electric fields, Phys. Rev. B **79**, 155308 (2009).

[36] A. Chomette, B. Deveaud, A. Regreny, and G. Bastard, Observation of carrier localization in intentionally disordered Gaas/Gaalas superlattices, Phys. Rev. Lett. **57**, 1464 (1986).

[37] B. V. Olson, J. F. Klem, E. A. Kadlec, J. K. Kim, M. D. Goldflam, S. D. Hawkins, A. Tauke-Pedretti, W. T. Coon, T. R. Fortune, E. A. Shaner, and M. E. Flatté, Vertical hole transport and carrier localization in InAs/InAs$_{1-x}$Sb$_x$ type-II superlattice heterojunction bipolar transistors, Phys. Rev. Appl. **7**, 024016 (2017).

[38] S. K. Lyo and D. H. Huang, Multisublevel magnetoquantum conductance in single and coupled double quantum wires, Phys. Rev. B **64**, 115320 (2001).

[39] Y. Zhu, D. H. Huang, and S. Feng, Tunneling plasmon excitations in quasi-zero-dimensional superlattices composed of quantum dots, Phys. Rev. B **40**, 3169 (1989).

[40] S. Ono, Thermalization in simple metals: Role of electron-phonon and phonon-phonon scattering, Phys. Rev. B **97**, 054310 (2018).

[41] S. K. Lyo and D. H. Huang, Effect of electron-electron scattering on the conductance of a quantum wire studied with the Boltzman transport equation, Phys. Rev. B **73**, 205336 (2006).

[42] S. K. Lyo and D. H. Huang, Temperature-dependent magnetoconductance in quantum wires: Effect of phonon scattering, Phys. Rev. B **68**, 115317 (2003).

[43] D. H. Huang and G. Gumbs, Coupled force-balance and scattering equations for nonlinear transport in quantum wires, Phys. Rev. B **80**, 033411 (2009).

[44] D. H. Huang, T. Apostolova, P. M. Alsing, and D. A. Cardimona, High-field transport of electrons and radiative effects using coupled force-balance and Fokker-Planck equations beyond the relaxation-time approximation, Phys. Rev. B **69**, 075214 (2004).

[45] G. Gumbs and D. H. Huang, *Properties of Interacting Low-Dimensional Systems* (John Wiley & Sons, New York, 2011).

[46] A. Majumdar, L. P. Rokhinson, D. C. Tsui, L. N. Pfeiffer, and K. W. West, Effective mass enhancement of two-dimensional electrons in a one-dimensional superlattice potential, Appl. Phys. Lett. **76**, 3600 (2000).

[47] Y. A. Romanov, On the differential conductivity of semiconductor superlattices, Phys. Solid State **45**, 559 (2003).